**Title**
STUDY OP THE Y1 RESONANT AMPLITUDES BETWEEN 1660 AND 1900 MeV IN THE REACTION K~n - An-



**Author**
Smart, Wesley Mitchell.

**Publication Date**
1967-08-01

UCRL-17712

cy. 2

# University of California

# Ernest O. Lawrence Radiation Laboratory

STUDY OF THE $Y_1^*$ RESONANT AMPLITUDES BETWEEN 1660 AND 1900 MeV IN THE REACTION $K^-n \rightarrow \Lambda\pi^-$

Wesley Mitchell Smart

August 1967



Berkeley, California

## DISCLAIMER

UNIVERSITY OF CALIFORNIA

Lawrence Radiation Laboratory
Berkeley, California

AEC Contract No. W-7405-eng-48

# STUDY OF THE $Y_1^*$ RESONANT AMPLITUDES BETWEEN 1660 AND 1900 MeV IN THE REACTION $K^- n \rightarrow \Lambda\pi^-$

Wesley Mitchell Smart
(Ph. D. Thesis)

August 1967

# STUDY OF $Y_1^*$ RESONANT AMPLITUDES BETWEEN 1660 AND 1900 MEV IN THE REACTION $K^- n \rightarrow \Lambda\pi^-$

## Contents

# STUDY OF $Y_1^*$ RESONANT AMPLITUDES BETWEEN 1660 AND 1900 MEV IN THE REACTION $K^-n \rightarrow \Lambda\pi^-$

Wesley Mitchell Smart

Lawrence Radiation Laboratory
University of California
Berkeley, California

August 1967

## ABSTRACT

The Lawrence Radiation Laboratory 25-inch deuterium bubble chamber was exposed to a beam of $K^-$ mesons having laboratory momenta between 815 and 1105 MeV/c. The angular distributions and $\Lambda$ polarizations in the reaction $K^-n \rightarrow \Lambda\pi^-$ were measured in the center-of-mass energy interval 1660 to 1900 MeV. A partial-wave analysis of the angular distributions and polarizations from $K^-n \rightarrow \Lambda\pi^-$ and the total-cross-section data from $K^-p \rightarrow \Lambda\pi^\circ$ has yielded information on the quantum numbers, resonance parameters, and SU(3) assignments for four $Y_1^*$ resonances.

The spin-parity assignments for $Y_1^*(1765)$ and $Y_1^*(2030)$ have been confirmed, and the $Y_1^*(1765)$ mass, width, and $\Lambda\pi$ branching ratio have been measured as 1772 ±6 MeV, 129 ±17 MeV, and 0.15 ±.02 respectively. A tentative spin-parity assignment for $Y_1^*(1660)$ and $Y_1^*(1915)$ was also made.

The measurement of the relative signs of the product of the coupling constants, $g_{N\bar{K}Y}^* \, g_{\Lambda\pi Y}^*$, for the four resonant amplitudes has limited their possible assignments to SU(3) multiplets. The $Y_1^*(1765)$ can only be a member of the $\{10^*\}$ or the $\{8\}$ multiplets. If it is a member of the octet, the value of $\alpha$ (the D-F mixing parameter) must be either less than 1/2 or greater than 1. This SU(3) assignment for $Y_1^*(1765)$ is based on the assumption that $Y_1^*(2030)$ is a member of a $\{10\}$ multiplet.

# I. INTRODUCTION

Early total-cross-section measurements of $K^-$ on protons and neutrons by Cook et al.[1] and Chamberlain et al.[2] indicated an asymmetric peak in $K^-p$ at a center-of-mass (c.m.) energy of about 1800 MeV. It was speculated that this peak was caused by at least one resonance. A comparison of the $K^-p$ and $K^-n$ total cross sections suggested that this peak was caused mainly by an isotopic-spin-zero amplitude identified as $Y_0^*(1815)$. Later studies of the $K^-p$ effective mass distribution from the reaction $K^-n \rightarrow K^-\pi^-p$ at 1.51 BeV/c by Barbaro-Galtieri, Hussain, and Tripp[3] showed a peak tenatively identified as a resonance of mass 1765 MeV and width 60 MeV. By studying the angular distributions obtained earlier,[4] for $K^-p$ elastic and charge-exchange scattering in the 1800-MeV region Barbaro-Galtieri et al. suggested I = 1 for the resonance at 1765. This paper describes one of several experiments done to understand the details of $K^-$-nucleon interactions, particularly the resonances, in the region around 1800 MeV.

The Lawrence Radiation Laboratory (LRL) 25-inch deuterium bubble chamber was exposed to a separated $K^-$ beam of momenta 815 to 1105 MeV/c at the Bevatron. Approximately 250 000 pictures were taken. The reaction $K^-n \rightarrow \Lambda\pi^-$ was selected to study the $Y_1^*$ resonate amplitudes in the c.m. energy region 1660 to 1900 MeV covered by the data. To completely specify a resonance one must determine its quantum numbers -- baryon number, charge, hypercharge, isotopic spin, spin, and parity. The mass $E_R$, total width $\Gamma$, branching ratios in the various channels $x_c$, and the SU(3) assignment are also of interest.

The two-body final-state interaction $K^-n \rightarrow Y_1^* \rightarrow \Lambda\pi^-$ is particularly well-suited for determining these quantities for $Y_1^*$

resonances. The final state $\Lambda\pi$ has baryon number 1, charge -1, hypercharge 0, and isotopic spin 1; hence any resonance found in this interaction must have these quantum numbers. The initial state also has pure I = 1; thus any contamination from $K^-n \rightarrow \Sigma^\circ\pi^-$, $\Sigma^\circ \rightarrow \Lambda\gamma$ cannot come from an I = 0 resonance. The theory of partial-wave analysis, necessary to separate the various $J^P$ amplitudes, is well developed for this type of interaction. The parity-violating weak decay of the $\Lambda$ is an efficient analyzer for the $\Lambda$ polarization; this polarization information is vital for a complete partial-wave analysis to determine the spin and parity of a resonance. Since this is a reaction channel, measuring the relative phases of two or more resonant amplitudes yields information on their SU(3) assignments that is unavailable in the elastic or charge-exchange channels. Finally, since the $\pi^-$ track in $K^-n \rightarrow \Lambda\pi^-$ is visible in the bubble chamber, the problems of locating the production origin and eliminating $\Sigma^\circ$ background are reduced. The analysis of the reaction $K^-p \rightarrow \Lambda\pi^\circ$ suffers from these problems.

This paper describes the theory of partial-wave analysis, which is necessary to separate the various spin-parity amplitudes and to identify those which have resonant behavior; the background needed to understand the SU(3) classifications of the particles; and the experimental details, data processing, and the resulting distributions. The application of the partial-wave analysis to the reaction $K^-n \rightarrow \Lambda\pi^-$ and the resulting information on quantum numbers, resonance parameters, and SU(3) assignments for $Y_1^*(1660)$, $Y_1^*(1765)$, $Y_1^*(1915)$, and $Y_1^*(2030)$ complete the study.

At the time the preliminary results of this experiment were published,[5,6] the following information was known about the four $Y_1^*$

resonant amplitudes which might be present in the energy interval under study:

$Y_1^*(1660)$. This resonance has $J = 3/2$, $E_R = 1660$ MeV, $\Gamma \cong 44$ MeV, $x_{N\bar{K}} \cong 0.15$, and $x_{\Lambda\pi} \cong 0.05$.[7] The branching ratio in channel C, $x_C$ is equal to the ratio of the partial width $\Gamma_C$ in channel C to the total width $\Gamma$. The parity is uncertain.

$Y_1^*(1765)$. This resonance had $E_R \cong 1762$ MeV, $\Gamma \cong 75$ MeV, and $x_{N\bar{K}} \cong 0.5$. No value for $x_\pi$ had been published. The assignment I $J^P = 1, 5/2^-$ had been deduced from studies of the reaction $K^-N \rightarrow Y_0^*(1520) + \pi$ by Armenteros et al. and Bell et al.[8]

$Y_1^*(1915)$. This effect was discovered as a shoulder in the $K^-n$ total cross section as measured by Cool et al.[9] The shoulder is consistent with a resonance with $E_R = 1915$ MeV, $\Gamma = 65$, and $(J + 1/2)\, x_{N\bar{K}} = 0.31$, but J, P, and $x_{\Lambda\pi}$ are unknown.

$Y_1^*(2030)$. A study of the reactions $K^-p \rightarrow \Lambda\pi^\circ$ and $K^-p \rightarrow \bar{K}^\circ n$ in the $K^-$ momentum interval 1220 to 1700 MeV/c has given I, $J^P = 1, \frac{7}{2}^+$ with $x_{N\bar{K}} = 0.25$ and $x_{\Lambda\pi} = 0.15$ for this resonance.[10]

The emphasis in this experiment has been to measure or confirm the quantum numbers, resonance parameters, and SU(3) assignments for the above four resonances. In addition, the nonresonant partial-wave amplitudes in the reaction $K^-n \rightarrow \Lambda\pi^-$ have been measured approximately.

A partial-wave analysis of the angular distributions and polarizations in the reaction $K^-n \rightarrow \Lambda\pi^-$ and using the published total cross sections for $K^-p \rightarrow \Lambda\pi^\circ$ leads to the following results: The parity of $Y_1^*(1660)$ is probably negative; a conclusive parity determination is not possible because the $Y_1^*(1660)$ amplitude is relatively weak in the $\Lambda\pi$ channel and there is insufficient data around

1660 MeV in this experiment. There are some indications that $J^P = \frac{5}{2}^+$ and $x_{\Lambda\pi} = 0.16 \pm .12$ for $Y_1^*(1915)$. This spin-parity assignment would make $Y_1^*(1915)$ a candidate for the Regge recurrence of the $\Sigma$ hyperon.

$Y_1^*(2030)$. We verify that the I, $J^P$ assignment for $Y_1^*(2030)$ is $1, \frac{7}{2}^+$.

$Y_1^*(1765)$. The dominate feature in the reaction $K^-N \rightarrow \Lambda\pi$ between 1660 and 1900 MeV is this resonance. We measure $E_R = 1772 \pm 6$ MeV, $\Gamma = 129 \pm 17$, $x_{\Lambda\pi} = 0.15 \pm .02$, and I, $J^P = 1, 5/2^-$, confirming the previous I $J^P$ assignment.[8]

SU(3) Assignments. Measuring the relative phases of the four resonance amplitudes leads to restrictions on their assignments to SU(3) multiplets.

Finally, this study has demonstrated the advantages in analyzing reaction-channel data with an energy-dependent partial-wave analysis even with a rather modest amount of data available at each energy.

# II. THEORY

## A. Partial-Wave Analysis

The reaction $K^-n \rightarrow \Lambda\pi^-$ is one of a large class called formation experiments, in which a resonant amplitude is excited when the c.m. energy of the $K^-n$ system corresponds to the energy of the resonance. If other amplitudes are small compared to the resonant amplitude, its existence is clearly demonstrated by the rise and fall of the total cross section as a function of energy for the reaction. Unfortunately, in the channel $K^-n \rightarrow \Lambda\pi^-$ the nonresonant amplitudes are not small, and a more detailed examination of the angular distributions and polarizations must be made to determine the mass, width, and branching ratio of the resonance. Also the total cross section gives only a lower limit for the spin and no information on the parity of the resonance.

To obtain the more complete information available in a formation experiment, it is necessary to measure the angular distributions and polarizations of the final baryon in addition to the total reaction cross section and then decompose the amplitude into partial-wave amplitudes, i.e. eigenstates of angular momentum and parity. A more comprehensive discussion of the theory of partial-wave analysis in formation experiments can be found in an article by Tripp.[11]

In a reaction with spin 0 + spin 1/2 goes to spin 0 + 1/2 (such as $K^-n \rightarrow \Lambda\pi^-$) the transition operator M is given by

$$M = a\ (\theta) + b\ (\theta)\ \vec{\sigma} \cdot \hat{n}.$$

There are two amplitudes: a, the non-spin-flip, and b, the spin-flip amplitude. If we define $\hat{K}$ to be a unit vector along the incident $K^-$ c.m. momentum and $\hat{\pi}$ along the final $\pi^-$ c.m. momentum, the a and b amplitudes are functions of $\theta$ ($\cos\theta = \hat{K} \cdot \hat{\pi}$); $\sigma$ is the Pauli spin

operator, and $\hat{n} = (\hat{K} \times \hat{\pi})/(|\hat{K} \times \hat{\pi}|)$ is the normal to the production plane. The relations between $a(\theta)$ and $b(\theta)$ and the complex partial-wave amplitudes $T_\ell^{\pm}$ ($\ell$ is the final orbital angular momentum, $J = \ell \pm 1/2$) are

$$a(\theta) = \lambda\!\!\!^{-} \sum_\ell \left[ (\ell + 1) T_\ell^{+} + \ell T_\ell^{-} \right] P_\ell (\cos \theta) \tag{1a}$$

and

$$a(\theta) = i\lambda\!\!\!^{-} \sum_\ell \left[ T_\ell^{+} - T_\ell^{-} \right] P_\ell^{1} (\cos \theta), \tag{1b}$$

where $\lambda\!\!\!^{-}$ is the incident c.m. wave length divided by $2\pi$, $P_\ell$ is the $\ell$ th order Legendre polynomial, and $\vec{P}_\ell^{\,1}$ is the first associated Legendre polynomial. The differential cross section I and polarization $\vec{P}$ are given in terms of a and b by

$$I = \frac{d\sigma}{d\Omega} = |a|^2 + |b|^2 \tag{2a}$$

and

$$I\vec{P} = 2 \, \mathrm{Re} \, (a^* b) \, \hat{n}. \tag{2b}$$

The polarization is restricted to be along $\hat{n}$ by parity conservation in strong interactions. In order to obtain a more direct relation between the measured distribution I and $I\vec{P}$ and the partial-wave amplitudes, it is customary to make the expansion

$$I = \lambda\!\!\!^{-2} \sum_{m=0} A_m P_m (\cos \theta) \tag{3a}$$

and

$$I\vec{P} = n \, \lambda\!\!\!^{-2} \sum_{n=1} B_n P_n^{1} (\cos \theta) \tag{3b}$$

and then refer to tables[11,12] relating the A and B coefficients to the partial-wave amplitudes $T^{\pm}$. Table I is useful in converting between the various notations used. The parity P of the two-particle system in the final state has been calculated from $P = (-1)^\ell P_B P_M = -(-1)^\ell$ for the usual case of a pseudoscalar meson M and even-parity baryon B.

The variation with c.m. energy of the partial-wave amplitudes is,

Table I. Various notations used for partial wave amplitudes. The parity, P, of the two particle system in the final state has been calculated from $P = (-1)^{\ell} P_B P_M = -(-1)^{\ell}$ for the usual case of a pseudoscalar meson, M, and even parity baryon, B.

| $T_{\ell}^{\pm}$ | $T_0^+$ | $T_1^-$ | $T_1^+$ | $T_2^-$ | $T_2^+$ | $T_3^-$ | $T_3^+$ | $T_4^-$ | $T_4^+$ |
|---|---|---|---|---|---|---|---|---|---|
| $\ell 2J$ | S1 | P1 | P3 | D3 | D5 | F5 | F7 | G7 | G9 |
| $J^P$ | $\frac{1}{2}^-$ | $\frac{1}{2}^+$ | $\frac{3}{2}^+$ | $\frac{3}{2}^-$ | $\frac{5}{2}^-$ | $\frac{5}{2}^+$ | $\frac{7}{2}^+$ | $\frac{7}{2}^-$ | $\frac{9}{2}^-$ |

in general, unknown. However, in the special case of a resonant amplitude, it is governed by the Breit-Wigner formula

$$T = \frac{\frac{1}{2}(\Gamma_e \Gamma_r)^{1/2}}{(E_R - E) - i\Gamma/2}, \tag{4}$$

where E is the c.m. energy, $E_R$ the energy of the resonance, $\Gamma_e$ the partial width in the incident (elastic) channel, $\Gamma_r$ the partial width in the final (reaction) channel, and $\Gamma = \sum_{ii} \Gamma$, where the summation is over all decay channels of the resonance. The energy dependence of the partial widths has been approximated as

$$\Gamma_i \propto \left[\frac{q_i^2}{q_i^2 + X^2}\right]^{\ell_i} \frac{q_i}{E} \tag{5}$$

by Glashow and Rosenfeld,[13] where X is a mass related to the radius of interaction and $q_i$ and $\ell_i$ are the momentum and orbital angular momentum of the decay products of the resonance in the i th channel. Glashow and Rosenfeld found X = 350 MeV from a study of the SU(3) predictions for the partial widths of the $\gamma$ ($J^P = 3/2^-$) octet.[13] Deans and Holladay found that X = 175 MeV gives a better fit to the $\Delta$ (1236) resonance.[14] Blatt and Weisskopf[15] derive (nonrelativistically) an expression for the energy dependence of $\Gamma_i$ which is identical in form with Eq. (5) for $\ell = 1$, but differs somewhat for higher $\ell$ values. For this study the Glashow and Rosenfeld form [Eq. (5)] has been used, with X fixed at 350 MeV.

A careful study of Eq. (1) and (2) shows that the transformation $T_\ell^+ \rightarrow T_{\ell+1}^-$, $T_\ell^- \rightarrow T_{\ell-1}^+$ (i.e. changing the parities of all amplitudes) leaves I invariant but changes the sign of $\vec{P}$. Also the transformation $T_\ell^\pm \rightarrow T_\ell^{\pm *}$ has the same effect. The first is called the Minami transformation; the second is the complex-conjugation transformation.

Measuring the polarization removes two of the four possibilities, but additional information is required to completely specify the solution. Making measurements at several energies and then applying the Wigner condition[12] to a resonant amplitude is sufficient to remove the ambiguity. This condition requires rapidly varying resonant amplitudes to traverse the complex plane in a counterclockwise direction and is implicit in Eq. (4). Figure 1 is an Argand diagram, which displays the energy behavior of a partial-wave amplitude in the complex plane. Note that there are two possible trajectories for a resonant amplitude, depending on the sign of the numerator in Eq. (4). The implication of this difference will be discussed below. The circle at radius 0.5 is the unitary limit for partial-wave amplitudes in a reaction channel.

Equations (1) and (2) also show that I and $I\vec{P}$ are invariant under the transformation $T_\ell^{\pm} \rightarrow e^{i\varphi} T_\ell^{\pm}$. In the elastic channel this degeneracy is removed by the optical theorem

$$\text{Im } a\ (0^\circ) = \frac{k}{4\pi}\ \sigma_T\ ,$$

which relates the imaginary part of the forward-scattering amplitude to the total cross section. However no such relation exists for an inelastic channel, so that the degeneracy is usually taken into account by defining the phase of one of the partial-wave amplitudes.

At one energy there is sufficient information in the experimental distributions I and $I\vec{P}$ to just determine all the partial waves (but not to resolve the ambiguity discussed above, or to remove the degeneracy in the inelastic channels). If only the first n partial waves are present, then the expansions (3) require terms up to order (n-1).[11,12] One must determine 2n quantities to describe the n complex partial waves. The differential cross section I provides n ($A_0$, $A_1$ ..., $A_{n-1}$)

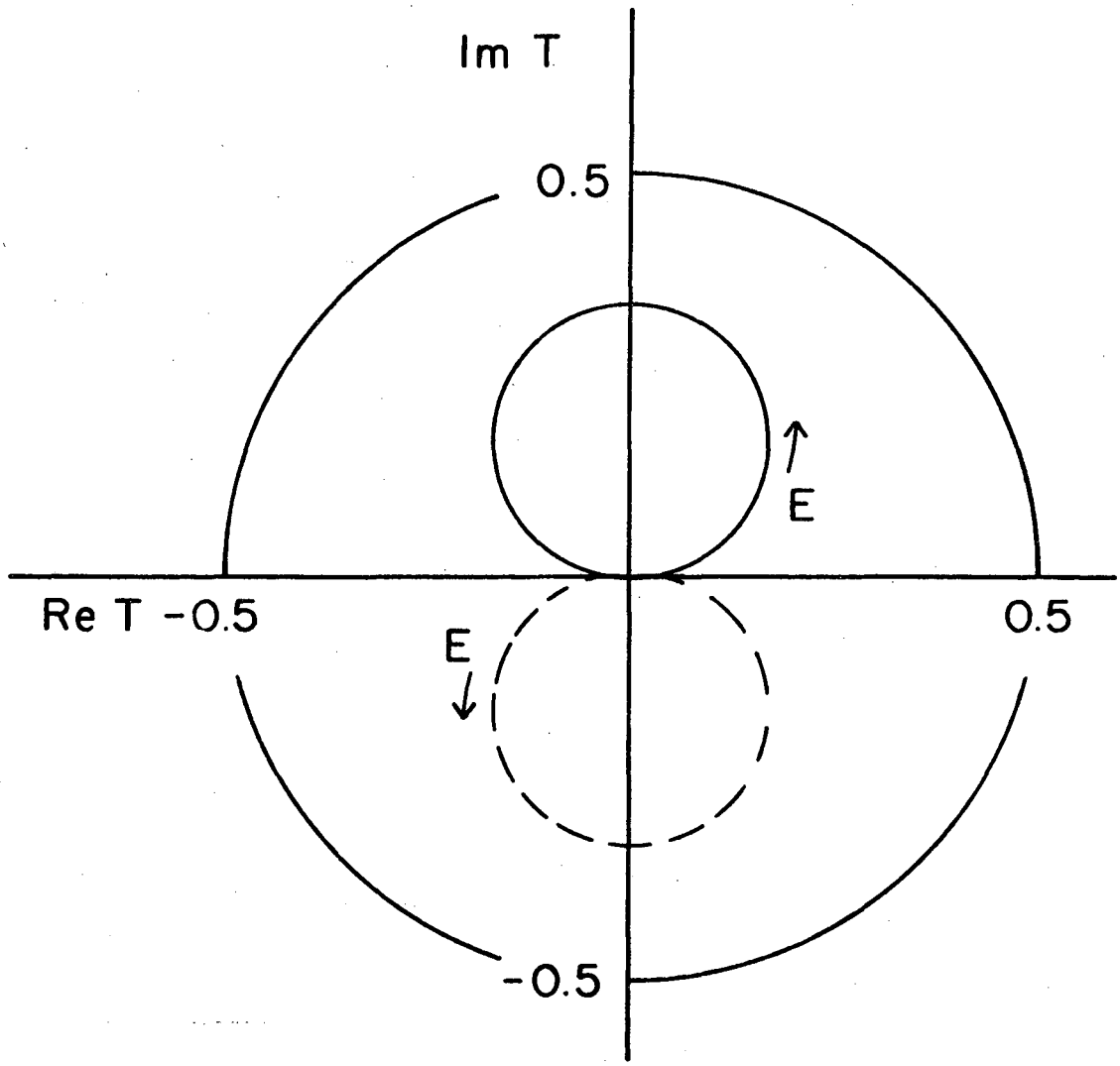


XBL 678-4483

Fig. 1. Argand diagram for a resonant partial wave amplitude in a reaction channel. The circle at radius 0.5 is the unitary limit.

of these quantities, and the polarization measures n-1 ($B_1$, $B_2$, ..., $B_{n-1}$) more. For the elastic channel the optical theorem provides the remaining relationship to completely determine the n partial waves; for the inelastic channels the one undetermined parameter corresponds to the overall phase degeneracy. Since precise data, particularly for the polarization, is often not available, one must make assumptions to reduce the number of free parameters to be determined from the data. The assumptions made in this experiment will be discussed in Section 6A.

## B. SU(3)

Since Gell-Mann[16] and Ne'eman[17] made the correspondence between the eight $J^P = 1/2^+$ Baryons (p, n, $\Sigma^+$, $\Sigma^\circ$, $\Sigma^-$, $\Lambda$, $\Xi^\circ$, $\Xi^-$) and the octet represnetation of the special symmetry group of three dimensions, the SU(3) assignment for other particles has been of interest. This subsection describes how the measurement of the relative phase of resonance amplitudes restricts their possible SU(3) assignments.[18] Representations of SU(3) correspond to groupings of particles with the same baryon number, spin, and parity. Hypercharge Y, isotopic spin, and the Z component of isotopic spin $I_Z$ vary among the members of each representation. Thus it is convenient to display the representations by a plot of Y vs $I_Z$ for each member. Figure 2 shows these plots for the possible representations of SU(3) which are of interest for this experiment.

Both the spin 0, negative parity mesons M ($K,\pi,\eta,\bar{K}$) and the spin 1/2, positive parity baryons B ($N,\Sigma,\Lambda,\Xi$) are assigned to an octet $\{8\}$ representation of SU(3), and this is indicated by the notation to the right of Fig. 2a. According to the algebra of SU(3) only a particle assigned to the representations $\{27\}$, $\{10^*\}$, $\{10\}$, $\{8\}$, or $\{1\}$ can

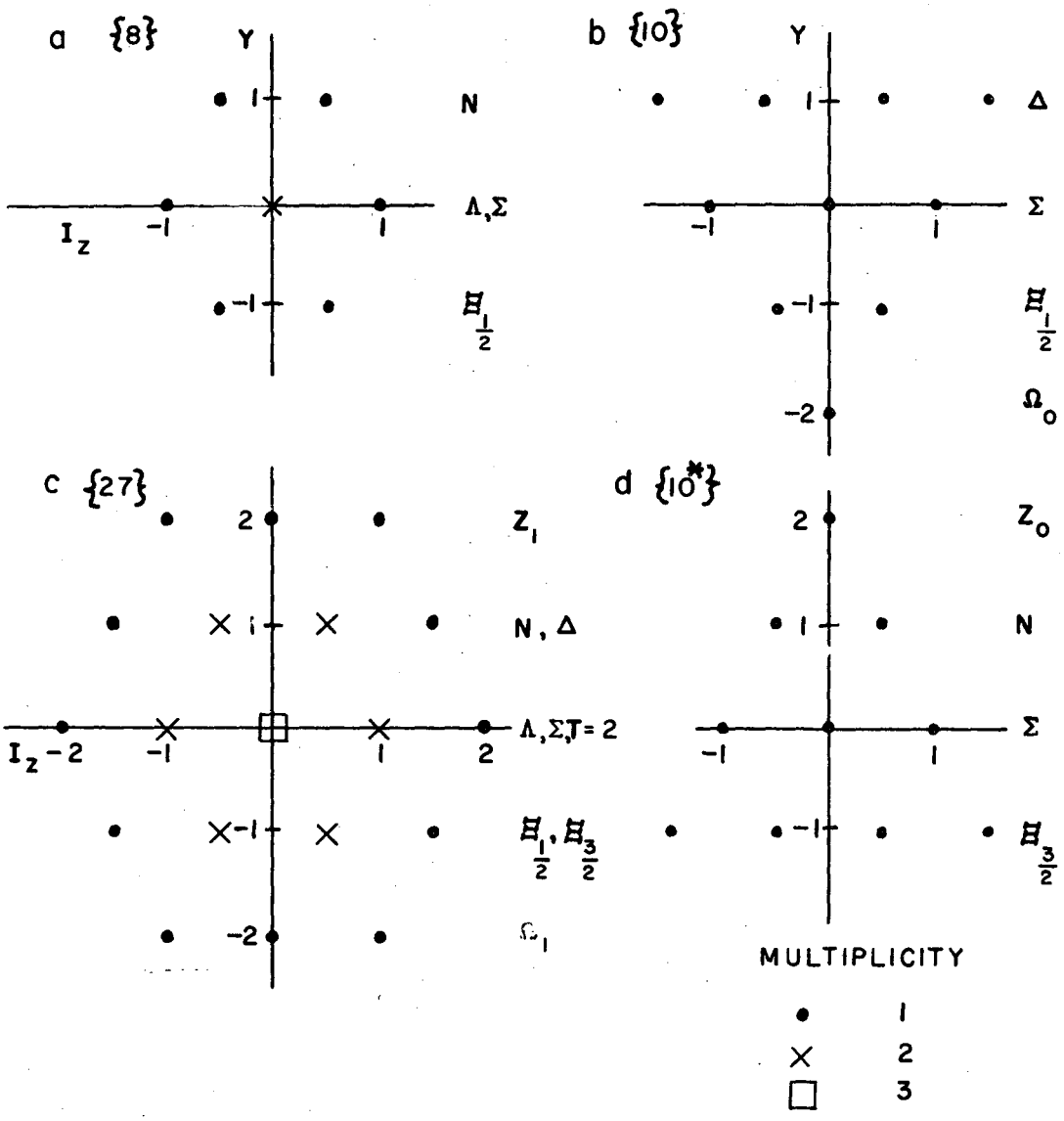


Fig. 2. Representations of SU(3) which are of interest for this experiment.

decay into two particles each belonging to an octet:[19]

$$\{8\} \otimes \{8\} = \{27\} \oplus \{10\} \oplus \{10^*\} \oplus \{8_1\} \oplus \{8_2\} \oplus \{1\} . \quad (6)$$

The reaction $K^- n \rightarrow Y_1^{*-} \rightarrow \Lambda\pi^-$ can be represented by the diagram in Fig. 3, where $g_{nK^-Y^*}$ gives the coupling at the production vertex, and $g_{\Lambda\pi^-Y^*}$ gives the coupling at the decay vertex. Since the square of the coupling constant is proportional to the partial width, we may rewrite Eq. (4), for the resonant partial-wave amplitude

$$T \propto \frac{g_{N\bar{K}Y}^* \, g_{\Lambda\pi Y}^*}{(E_R - E) - i\Gamma/2} . \quad (7)$$

The sign of the numerator is determined by the product of the signs of the coupling constants. These signs are predicted by the SU(3) assignment for a $Y_1^*$. The coupling constant $g_{BMY}^*$ may be written

$$g_{BMY}^* = C g_\mu , \quad (8)$$

where C is a SU(3) Clebsch-Gordan coefficient that depends on the hypercharge, isotopic spin, z component of isotopic spin, and multiplet assignment for each of the three particles at a vertex. The coupling constant $\{g_\mu\}$ is the overall strength for the decay of a member of a multiplet $\{\mu\}$ into two octets and is not predicted by SU(3). The sign of $g_\mu$ is unimportant, because only $g_\mu^2$ enters into Eq. (7). Hence the sign of the numerator of Eq. (7) is determined by the sign of the product of the two appropriate SU(3) Clebsch-Gordan coefficients. Table II gives the necessary Clebsch-Gordan coefficients for this experiment.[20] For an octet there are two coupling constants $g_1$ and $g_2$ because two $\{8\}$'s are contained in $\{8\} \otimes \{8\}$ (Eq. 6). These are rewritten in the notation of de Swart[4] as $g_8$ and $\alpha$, where $g_8 = (\sqrt{30}/40)\, g_1 + (\sqrt{6}/24)\, g_2$ and $\alpha = (\sqrt{6}/24)\, g_2/g_8$.

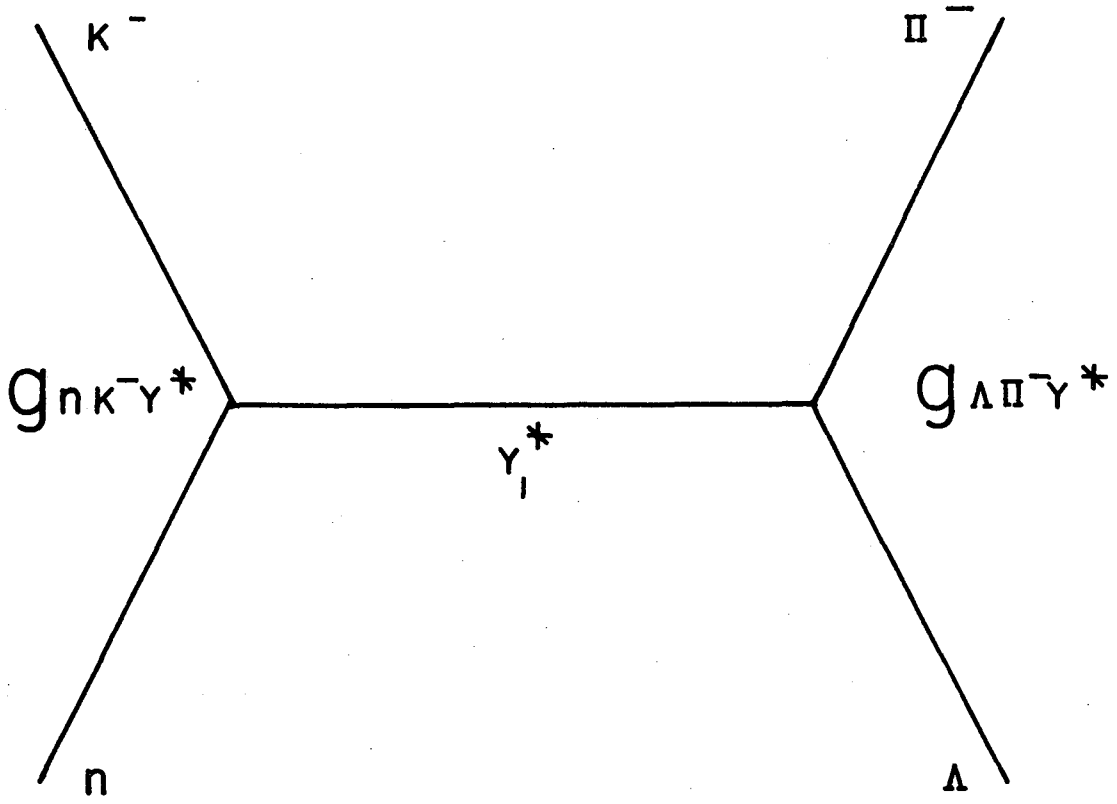


XBL 678-4485

Fig. 3. Diagram for the reaction $K^-n \rightarrow Y_1^* \rightarrow \Lambda\pi^-$. The coupling at the production vertex is given by $g_{nK^-Y^*}$ and $g_{\Lambda\pi^-Y^*}$ is the coupling at the decay vertex.

Table II. SU(3) Clebsch-Gordan coefficients for the decomposition of $|\mu, Y, I, I_3\rangle = |\mu, 0, 1, -1\rangle$ into $|8, y, i, i_3\rangle \otimes |8, y', i', i_3'\rangle$.

$Y_1^{*-}$

| $\{\mu\}$ | $\{27\}$ | $\{10\}$ | $\{10^*\}$ | $\{8_1\}$ | $\{8_2\}$ | $\{8\}$ |
|---|---|---|---|---|---|---|
| Y | 0 | 0 | 0 | 0 | 0 | 0 |
| I | 1 | 1 | 1 | 1 | 1 | 1 |
| $I_3$ | -1 | -1 | -1 | -1 | -1 | -1 |

| | $y$ | $i$ | $i_3$ | $y'$ | $i'$ | $i_3'$ | | | | | | |
|---|---|---|---|---|---|---|---|---|---|---|---|---|
| $nK^-$ | 1 | $\frac{1}{2}$ | $-\frac{1}{2}$ | -1 | $\frac{1}{2}$ | $-\frac{1}{2}$ | $\sqrt{1/5}$ | $-\sqrt{1/6}$ | $\sqrt{1/6}$ | $-\sqrt{3/10}$ | $\sqrt{1/6}$ | $-\sqrt{16}(1-2\alpha)$ |
| $\Sigma^0\pi^-$ | 0 | 1 | 0 | 0 | 1 | -1 | 0 | $\sqrt{1/12}$ | $-\sqrt{1/12}$ | 0 | $\sqrt{1/3}$ | $\sqrt{32}\,\alpha$ |
| $\Sigma^-\pi^0$ | 0 | 1 | -1 | 0 | 1 | 0 | 0 | $-\sqrt{1/12}$ | $\sqrt{1/12}$ | 0 | $-\sqrt{1/3}$ | $-\sqrt{32}\,\alpha$ |
| $\Sigma^-\eta$ | 0 | 1 | -1 | 0 | 0 | 0 | $\sqrt{3/10}$ | $\sqrt{1/4}$ | $\sqrt{1/4}$ | $\sqrt{1/5}$ | 0 | $\sqrt{32/3}(1-\alpha)$ |
| $\Lambda\pi^-$ | 0 | 0 | 0 | 0 | 1 | -1 | $\sqrt{3/10}$ | $-\sqrt{1/4}$ | $-\sqrt{1/4}$ | $\sqrt{1/5}$ | 0 | $\sqrt{32/3}(1-\alpha)$ |
| $\Xi^-K^0$ | -1 | $\frac{1}{2}$ | $-\frac{1}{2}$ | 1 | $\frac{1}{2}$ | $-\frac{1}{2}$ | $\sqrt{1/5}$ | $\sqrt{1/6}$ | $-\sqrt{1/6}$ | $-\sqrt{3/10}$ | $-\sqrt{1/6}$ | $-\sqrt{16}$ |

Table III gives the product $g_{N\bar{K}Y}^* g_{BMY}^*$ for the various SU(3) assignments for the $Y_1^*$ and for the several channels. One can divide the possible SU(3) assignments into one group where $g_{N\bar{K}Y}^* g_{BMY}^*$ is positive and another where it is negative. By a partial-wave analysis, one can experimentally divide the various resonant amplitudes into two groups, differing in phase by 180 deg. To resolve the overall experimental phase ambiguity, one must use other information to assign one of the resonances to an SU(3) multiplet. Then the possible assignments for the others are restricted by the measurement of their relative phase.

It is possible to use Eq. (8) to deduce SU(3) assignments based on the experimentally measured branching ratios for a resonance into various channels. A kinematic factor, such as Eq. (5) must be included to account for the mass splitting in SU(3) multiplets. Because this experiment measures only the product of $N\bar{K}$ and $\Lambda\pi$ branching ratios, we have not attempted to use this method. Recent studies by Uhlig et al.[21] and Tripp et al.[22] as well as the earlier study by Glashow and Rosenfeld[13] have used experimentally measured branching ratios to deduce SU(3) assignments.

Table III. The quantity $g_{NKY}^{*}\, g_{BMY}^{*}$ for $Y_1^{*}$ a member of a $\{27\}$, $\{10\}$, $\{10^{*}\}$, or $\{8\}$ multiplet; B and M denote members of the $J^P = 1/2^+$ baryon octet and of the pseudoscalar meson octet respectively.

| B, M | $\{27\}$ | $\{10\}$ | $\{10^{*}\}$ | $\{8\}$ |
|---|---|---|---|---|
| $\Sigma^0\pi^-$ | 0 | $-g_{10}^2\sqrt{1/72}$ | $-g_{10}^{2*}\sqrt{1/72}$ | $-g_8^2\sqrt{512}\alpha(1-2\alpha)$ |
| $\Sigma^-\pi^0$ | 0 | $g_{10}^2\sqrt{1/72}$ | $g_{10}^{2*}\sqrt{1/72}$ | $g_8^2\sqrt{512}\alpha(1-2\alpha)$ |
| $\Sigma^-\eta$ | $g_{27}^2\sqrt{3/50}$ | $-g_{10}^2\sqrt{1/24}$ | $g_{10}^{2*}\sqrt{1/24}$ | $-g_8^2\sqrt{512/3}(1-\alpha)(1-2\alpha)$ |
| $\Lambda\pi^-$ | $g_{27}^2\sqrt{3/50}$ | $g_{10}^2\sqrt{1/24}$ | $-g_{10}^{2*}\sqrt{1/24}$ | $-g_8^2\sqrt{512/3}(1-\alpha)(1-2\alpha)$ |
| $\Xi^-K^0$ | $g_{27}^2\sqrt{1/25}$ | $-g_{10}^2\sqrt{1/36}$ | $-g_{10}^{2*}\sqrt{1/36}$ | $g_8^2\sqrt{256}(1-2\alpha)$ |

## III. EXPERIMENTAL DETAILS

### A. Beam Description

A two-stage separated $K^-$ beam was built and operated at the LRL Bevatron and directed into the 25-in deuterium bubble chamber. A more detailed description of the beam can be found in UCRL-11527.[23] The beam utilized the external proton beam with an external target for the following advantages: (a) production of $K^-$ at 0 deg and large solid-angle acceptance for increased $K^-$ flux, (b) short total beam length for reduced $K^-$ losses due to decay, and (c) independence from the magnetic field of the Bevatron for a wider range of possible beam momenta. Two high-voltage parallel-plate velocity spectrometers and their associated mass-separation slits reduced pion and muon contamination to less than 5% at beam momenta of 1015 MeV/c and below, and 9% at 1110 MeV/c. Two bending magnets and the first mass slit limited the total momentum bite to 2%. The beam was designed so that its horizontal width matched the bubble chamber thin entrance window and that the tracks were parallel in the bubble chamber.

### B. Beam Normalization

A total of 250 000 pictures were taken, distributed among four different beam momenta. Because of the smearing effect of the Fermi momentum of the neutron in the deuteron, the exposure gave a continuous distribution of $K^-n$ c.m. energies between 1660 and 1900 MeV. Table IV gives the pertinent information for each of the four beam momenta.

The average number of tracks per frame was determined by counting beam tracks in every fiftieth frame. A template was used to eliminate tracks outside the horizontal limits of the chamber thin window or outside the limits on the azimuthal angle (±2 1/4 deg from the central

Table IV. Beam normalization for each of the four beam momenta.

| Beam momentum (MeV) (center of fiducial volume) | 814 | 910 | 1007 | 1106 |
|---|---|---|---|---|
| Number of frames | 22925 | 76928 | 62808 | 90950 |
| Counted tracks/frame (start of f.v.), $N_{BT}$ | 6.27 | 8.66 | 9.33 | 10.00 |
| Interactions/frame (in f.v.) $N_I$ | 1.00 | 1.19 | 1.31 | 1.23 |
| Contamination[24] (%) | 4.9 | 6.0 | 5.3 | 9.2 |
| % of counted tracks inside dip and window cuts (%) | 93.5 | 94.4 | 94.6 | 95.2 |
| Effective number of $K^-$ per frame | 5.11 | 7.12 | 7.64 | 8.05 |
| Total $K^-$ track length (km) | 47 | 220 | 196 | 295 |
| $\sigma_n$[25] (mb) | 33 | 41 | 40 | 34 |
| $\sigma_p$ (mb) | 40 | 44 | 48 | 45 |
| $\sigma_d$ (mb) | 68 | 78 | 82 | 75 |
| Screening correction factor, $f_g$ | 0.939 | 0.928 | 0.927 | 0.936 |
| Corrected total track length, L (km) | 44 | 205 | 182 | 276 |
| Cross section for one event ($\mu$b) | 5.54 | 1.199 | 1.352 | 0.889 |

value). Since the total $K^-d$ cross section had not been measured when the beam count was made, the number of beam tracks which interacted or decayed was also recorded. This number is needed to estimate the total $K^-$ track length.

The contamination of $\pi^-$ and $\mu^-$ in the beam was determined from a δ-ray count done in a companion hydrogen run with the same beam at the same momentum[24] and are shown in Table IV. The non-$K^-$ tracks were found to be 85% $\mu^-$ (which do not interact strongly), and the remainder were $\pi^-$. The effective number of $K^-$ tracks per frame was then approximately

$$(1 - C)\, N_{BT} - \frac{1}{2}\, N_I ,$$

where C is the contamination, $N_{BT}$ is the average number of beam tracks, and $N_I$ is the number of beam tracks which interact or decay. This number must be further corrected to allow for beam tracks that were outside the limits on dip angle (±2 deg) or the limits on vertical position at the chamber entrance. A track length of 40.3 cm was used. Multiplying this track length by the product of the number of frames and the effective number of $K^-$ per frame gives the total track length.

Since part of the time the neutron was screened behind the proton in the deutron the Glauber screening correction[9] had to be taken into account. For total neutron cross sections this correction is expressed by

$$\sigma_n = (\sigma_d - \sigma_p) \Big/ \left[1 - (4\pi)^{-1} \langle r^{-2} \rangle \sigma_p\right], \qquad (9)$$

where $\langle r^{-2} \rangle$ is the average of the inverse square of the separation of the nucleus in the deuteron, taken to be 0.0423 $mb^{-1}$.[9] Expression (9) neglects a term involving the product of the real parts of the Kn and Kp forward-scattering amplitudes. Equation (9) can be

rewritten

$$\sigma_n + \sigma_p = \sigma_d \left( 1 + (4\pi)^{-1} \langle r^{-2} \rangle \sigma_n \sigma_p / \sigma_d \right) .$$

This was taken to mean that the $K^-$ track length available for all interactions, including $K^- n \rightarrow \Lambda \pi^-$, had been reduced by a factor

$$f_g = \left[ 1 + (4\pi)^{-1} \langle r^{-2} \rangle \sigma_p \sigma_n / \sigma_d \right]^{-1} .$$

The recently measured total cross sections[25] required for this correction factor are shown in Table IV. The results of all the above corrections are shown as the "corrected total track length", L, in Table IV.

The cross section for one event is

$$\sigma = \frac{1}{nL} ,$$

where $n = N_A \rho$ is the number of neutrons per cubic centimeter in the bubble chamber. Here $\rho$ is the neutron density (measured as 0.0676 in this chamber[26]), and $N_A$ is Avagadro's number. The total cross section for any particular reaction in this experiment was determined by multiplying the number of events found by the cross section for one event. Because of the smearing effect of the Fermi momentum of the neutron in the deuteron, this cross section was actually an average over approximately 100 MeV c.m. energy.

## C. Scanning

The deuteron is a loosely bound system of a proton and a neutron; each baryon having a momentum distribution that can be calculated approximately from the Hulthen wave function. The impulse approximation considers that the interaction takes place with one baryon, the other being a spectator left with the momentum it had at the moment of impact. This approximation is expected to break down when the spectator has too

large a momentum, i.e. a small separation between the neutron and proton. An upper limit of 230 MeV/c was choosen for the spectator momentum in this experiment. The range for a 230 MeV/c proton in the bubble chamber was 6 cm. Each frame was scanned for the interaction sequence

$$\begin{aligned} K^- d &\rightarrow \Lambda^\circ \pi_1^- (p_1) \\ \Lambda^\circ &\rightarrow p\pi^- \quad , \end{aligned} \tag{10}$$

where $p_1$ is a spectator proton, i.e. less than 6 cm long. If $p_1$ was less than 1.5 mm long (85 MeV/c) the spectator proton track was ignored, as tracks shorter than this limit could not be measured by the methods used. Only one quarter of the events found had $p_1$ long enough to measure. If the V° had more than one possible production origin consistent with reaction (10), both were taken for measurement. The extraneous origin was removed by the bookkeeping process described in the next section. A total of 24 992 events were found. The efficiency, determined by scanning 24% of the film twice, was found to be 94.4%.

# IV. DATA PROCESSING

## A. Measuring

Approximately one fifth of the events were measured on the Flying Spot Digitizer (FSD), a computer-controlled automatic measuring machine. The remaining 20 029 events either had a visible spectator proton (which is too short for FSD measurement), lacked the special FSD fiducial or edge marks on the film, or failed two attempts at FSD measurement. These events were measured on the more conventional Franckenstein or measuring microscope. As the spectator proton was usually only a few millimeters long, its momentum could not be accurately measured by curvature in the magnetic field. However, since the spectator proton always stopped in the chamber, the range-momentum relations gave an accurate momentum measurement.

## B. Fog-Cloudy-Fair

After measurement by one of the methods outlined above, the events were processed through the system of computer programs FOG-CLOUDY-FAIR.[27] Using measurements from two of the three views of the bubble chamber, FOG reconstructs each track in space. CLOUDY constrains the reconstructed event to different hypotheses. For this experiment, origin 2 was tried as a decay from origin 1 (3 degrees of freedom) and both origins were fit together to the sequence (10). If the spectator is measured, only the magnitude of the $\Lambda$ momentum is unmeasured and this is a 7 C constraint; for unmeasured spectators the three components of the spectator momentum were also treated as unknown, making a 4 C fit. FAIR makes any desired cuts on the various quantities associated with each event and produces histograms, plots, lists, or computer tapes for further analysis.

## C. Bookkeeping

Because some 25 000 events were found by the scanning and because they were measured by a variety of methods over a prolonged period, it was necessary to establish a bookkeeping procedure, both to ensure that most of the events reached the final analysis and to obtain an accurate estimate of the percentage of events lost in the system in order to correct the cross section measurements. The information on each event found by the scanners was punched on IBM cards directly from the scan sheets. This information was compared by a FORTRAN computer program with a list of events completely processed through the system. In addition, events that had been inadverently measured twice were found, and the extra measurement eliminated from the final analysis. The incorrect combination of origins was eliminated for those pictures where the scanner was unsure of which $V_0$ came from which production origin. Events which were lost along the way were found and remeasured. It is estimated that without any bookkeeping at all 15 to 20 percent of the events would have been lost. By the procedures outlined above these losses were reduced to 1.9%.

## D. Event Selection

Events selected for final analysis were required to meet all the following criteria:

1. The incoming track had to lie within ±2 deg in dip and ±2 1/4 deg in azimuth of the average beam values for each momentum exposure. This was necessary to eliminate nonbeam tracks, as the average beam momentum was used rather than the less accurate measured value for each event.
2. The incoming track had to enter the chamber through the thin

window.

3. The $V_0$ had to have at least a 5% $\chi^2$ probability of being a $\Lambda$ from the production origin ($\chi^2 \leq 8$ for 3 degrees of freedom).
4. The two origins fitted together had to have a $\chi^2$ probability of at least 5% of being reaction (10) ($\chi^2 \leq 14.1$ for 7 degrees of freedom or $\chi^2 \leq 9.5$ for 4 degrees of freedom). In addition the constrained value of the spectator-proton momentum had to be less than 100 MeV for those events with unmeasured spectators.

Selections (1) and (2) also have been used in the beam normalization; hence no corrections are necessary. Selection (3) ideally should remove 5% of the events, however a study of the $\chi^2$ distribution indicated that about 7% of the events were removed by this cut. To estimate the number of $\Lambda\pi$ events remaining after the first three selections were made, the square of the missing mass at the first vertex was histogramed for events with measured and with unmeasured spectator protons at each beam momenta. These histograms were then fit to the sum of two Gaussian distributions -- one centered at the $\Lambda$ mass squared, and one at the $\Sigma^\circ$ mass squared. The width of the Gaussians, which is the experimental error in the missing mass squared, was varied for each histogram to obtain the best fit to the data. For those events with unmeasured spectators the centers of both the $\Lambda$ and $\Sigma^\circ$ Gaussians were also allowed to vary in the fits. The mass shifts necessary to obtain the best fits to the data were consistent with a rough calculation of the effect of ignoring the unmeasured spectator proton. The area under each Gaussian is then the number of $\Lambda\pi$ or $\Sigma^\circ\pi$ events in that histogram. The distributions are wider for the events with unmeasured spectators, because of the error introduced by ignoring the neutron momentum.

Figure 4a and b show these histograms and fitted curves for the measured and unmeasured spectator events at the 910 MeV/c beam momentum. The data for events at all four beam momenta appear in Table V.

In order to estimate the contamination from $\Sigma^\circ\pi$ in the events that met selection (4), the $\Lambda\pi$ Gaussian, normalized to the lower half at the $\Lambda\pi$ peak, was drawn on the missing-mass-squared histogram for the events meeting selection (4). The number of events above the Gaussian was taken to be the $\Sigma^\circ\pi$ contamination. The histograms are shown in Fig. 4c and d for the 910 MeV/c events, and these data for all momenta appear in Table V.

## E. Weighting

In order to ensure a reasonable probability that the $\Lambda$ decay could be observed and measured accurately, only beam tracks that interacted in the first 42 cm of the chamber were used. In addition the $K^-$ was required to go at least 2 cm into the chamber before interaction to permit a reasonable measurement of its angles. Because of curvature in the magnetic field the $K^-$ track length was 40.3 cm, slightly longer than the difference between the two figures above. This value of 40.3 cm was used in computing the total $K^-$ track length.

To permit accurate measurement of the $\Lambda$ decay tracks, the second origin was required to lie within a 15-cm-high cylinder of radius 21.5 cm centered 24.5 cm from the beam end of the chamber. This left at least 6 cm for the $\Lambda$ decay tracks. To ensure good detection efficiency the $\Lambda$ was also required to travel at least 3 mm before decay. To correct for events lost in these two cuts, each remaining event was assigned a weight $W_1$:

$$W_1 = (e^{-0.3/\bar{x}} - e^{-d/\bar{x}})^{-1} \quad ,$$

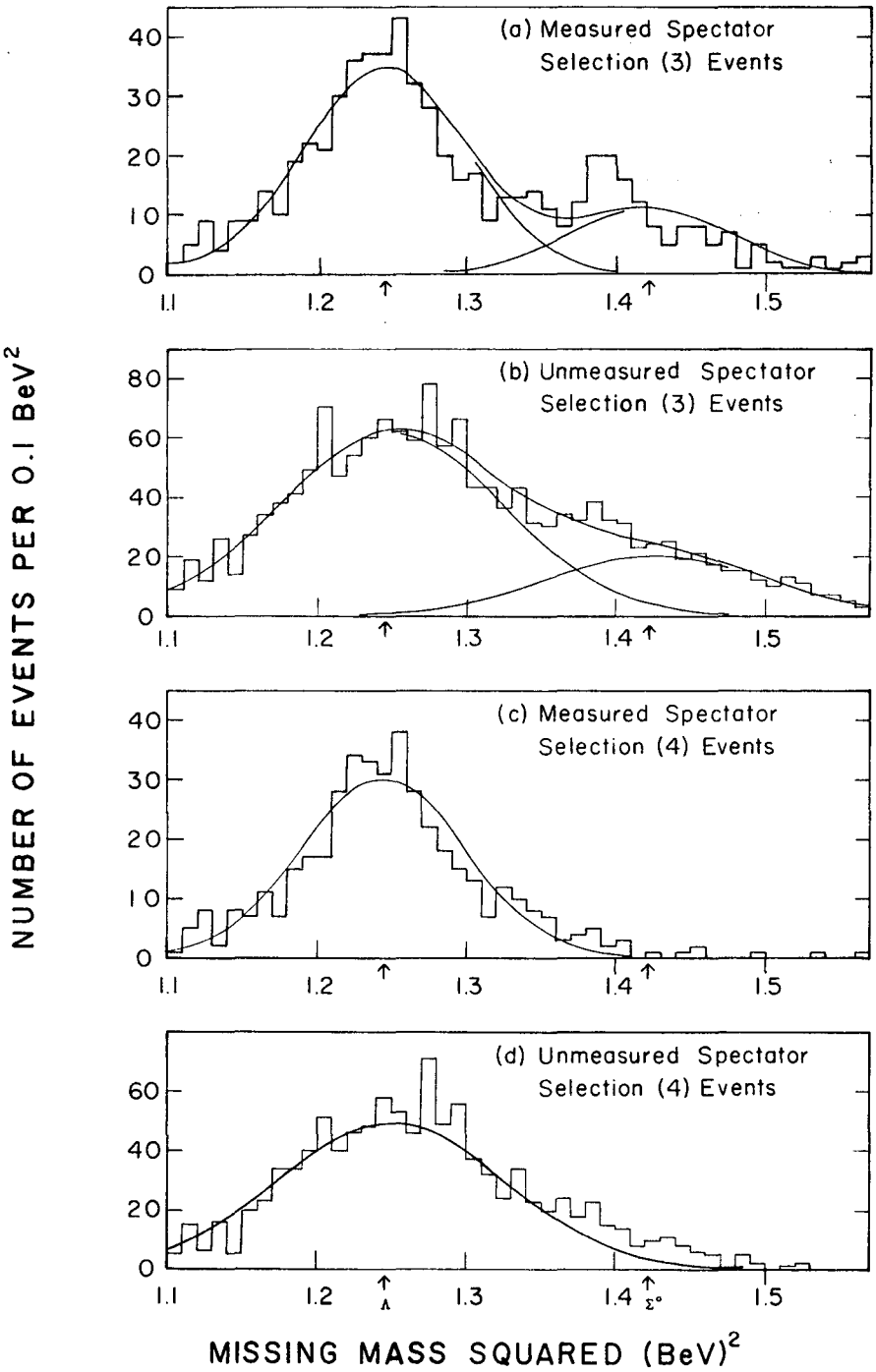


XBL 678-4494

Fig. 4. Experimental missing mass squared distribution and fitted curves for the events at the 910 MeV/c beam momentum.

Table V. Estimates of total number of $\Lambda\pi^-$ and $\Sigma^\circ\pi^-$ events meeting selection (3); estimates of $\Sigma^\circ\pi^-$ contamination in selection (4).

| Beam momentum (MeV) | 814 | 910 | 1007 | 1106 |
|---|---|---|---|---|
| Measured Spectators | | | | |
| Events under $\Lambda\pi$ curve | 122.3 | 478.1 | 331.6 | 446.2 |
| Events under $\Sigma\pi$ curve | 54.8 | 152.2 | 114.8 | 157.4 |
| Width of Gaussians ($BeV^2$) | 0.045 | 0.055 | 0.060 | 0.060 |
| $\chi^2/n$ | 18.8/16 | 48.9/41 | 51.8/39 | 52.9/44 |
| Confidence level (%) | 29 | 19 | 8 | 17 |
| $\Sigma\pi$ events meeting selection (4) | 15.5 | 9.4 | 9.4 | 36.5 |
| Percentage of selection (4) events which are $\Sigma\pi$ (%) | 12.6 | 2.2 | 3.1 | 8.7 |
| Percentage of $\Lambda\pi$ events cut by selection (4) (%) | 12.0 | 12.5 | 9.8 | 13.6 |

Table V. Continued

| Beam momentum (MeV) | 814 | 910 | 1007 | 1106 |
|---|---|---|---|---|
| | Unmeasured Spectators | | | |
| Events under $\Lambda\pi$ curve | 232.7 | 1156.7 | 945.8 | 1036.2 |
| Events under $\Sigma\pi$ curve | 127.7 | 383.6 | 283.6 | 363.9 |
| Width of Gaussians ($BeV^2$) | 0.060 | 0.075 | 0.085 | 0.080 |
| Fitted $\Lambda$ mass squared ($BeV^2$) | 1.250 | 1.250 | 1.265 | 1.265 |
| Fitted $\Sigma$ mass squared ($BeV^2$) | 1.437 | 1.427 | 1.437 | 1.437 |
| $\chi^2/n$ | 17.7/20 | 35.9/43 | 36.5/43 | 50.6/43 |
| Confidence level (%) | 62 | 77 | 78 | 20 |
| $\Sigma\pi$ events meeting selection (4) | 26.4 | 129.6 | 54.2 | 106.9 |
| Percentage of selection (4) events which are $\Sigma\pi$ (%) | 13.1 | 12.4 | 6.8 | 11.7 |
| Percentage of $\Lambda\pi$ events cut by selection (4) (%) | 24.1 | 19.2 | 19.5 | 20.9 |

Table V. Continued

| Beam momentum (MeV) | 814 | 910 | 1007 | 1106 |
|---|---|---|---|---|
| | All Events | | | |
| Events under $\Lambda\pi$ curves | 355.0 | 1634.8 | 1277.4 | 1482.4 |
| Events under $\Sigma\pi$ curves | 182.5 | 535.8 | 398.4 | 521.3 |
| $\Sigma\pi$ events meeting selection (4) | 41.9 | 139.0 | 63.6 | 143.4 |
| Percentage of selection (4) events which are $\Sigma\pi$ (%) | 12.9 | 9.5 | 5.8 | 10.8 |
| Percentage of $\Lambda\pi$ events cut by selection (4) (%) | 19.9 | 17.2 | 16.9 | 18.7 |

where d is the distance from the production origin to the boundary of the cylinder (potential path length), and $\bar{x} = \tau\, c\, P_\Lambda/m$ is the average length expected for a $\Lambda$ of momentum P. The $\Lambda$ mass was taken to be m = 1.1156 BeV, lifetime $\tau = 2.51 \times 10^{-10}$ sec, and c is the speed of light.[28]

The distribution, in the $\Lambda$ center of mass, of the cosine of the angle of the decay proton with respect to the $\Lambda$ line of flight should be isotropic. By studying this distribution one can correct for lambdas lost because of very-short decay proton lengths (low-momentum $\Lambda$) or short pion lengths (higher-momentum $\Lambda$). The weight $W_2$ was assigned according to:

| | |
|---|---|
| $W_2 = 1.08$ | $0 \leq P_\Lambda \leq 400$ MeV/c |
| $W_2 = 1.05$ | $400 \leq P_\Lambda \leq 800$ MeV/c |
| $W_2 = 1.07$ | $800 \leq P_\Lambda \leq 1200$ MeV/c |
| $W_2 = 1.04$ | $1200 \leq P_\Lambda$ |

as found by studying the distribution described above.

If one defines a polar coordinate system in the laboratory with the z axis along the beam direction, $\theta$ as the angle between the beam direction and the outgoing $\pi^-$, and $\varphi$ as the azimuthal angle with $\varphi = 0$ deg for $\pi^-$ in the plane containing the z axis and the camera axis and headed toward the camera, then the distribution of events in the angle $\varphi$ should be isotropic. These distributions are shown as the solid-line histograms in Fig. 5. Clearly events are being lost in the $\varphi = 0$ or 180 deg regions where the projected $K^-$, $\pi^-$ angle in the camera object plane $\beta$ is small. This bias was corrected by a factor $W_3$:

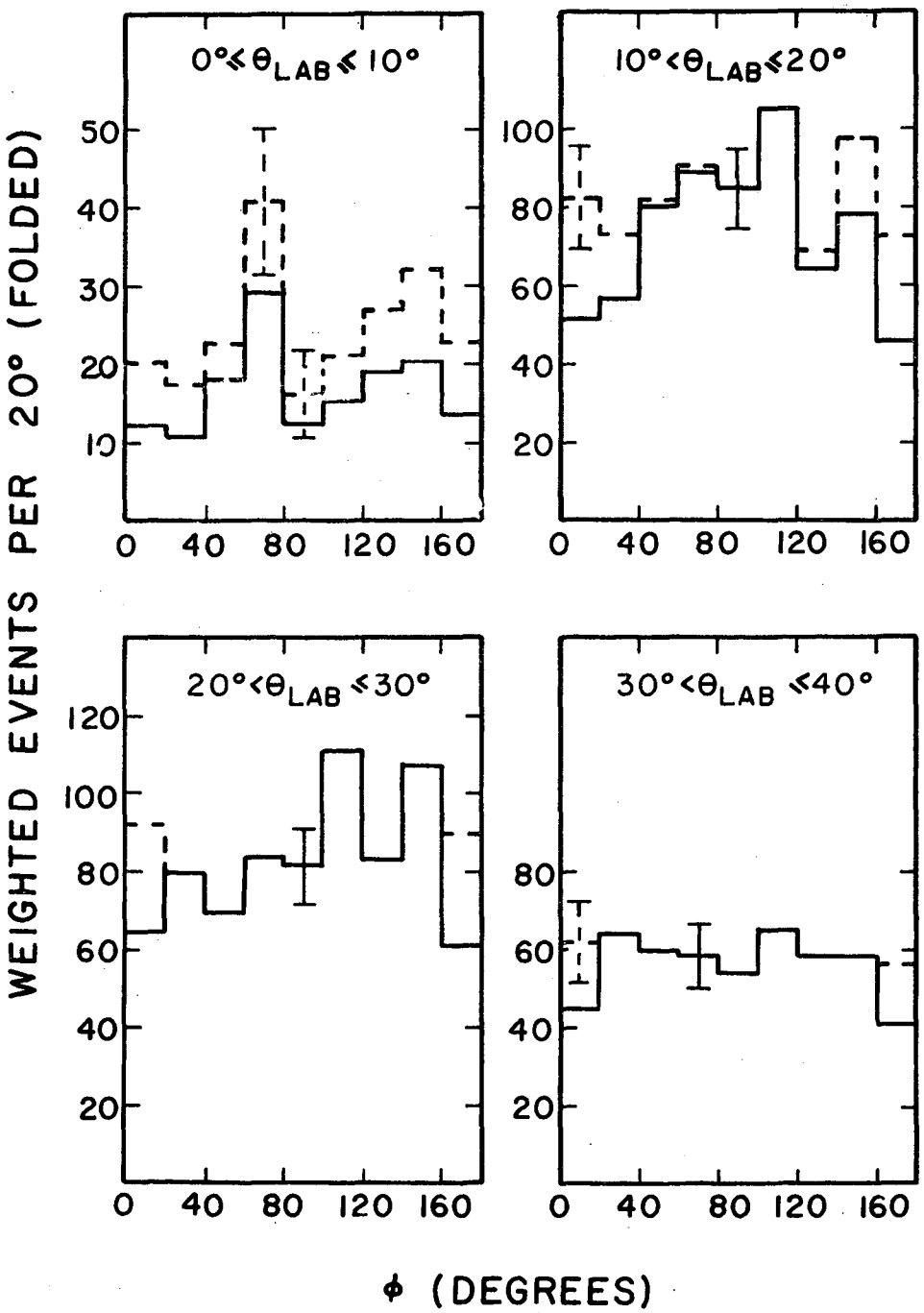


XBL 678-4486

Fig. 5. Azimuthal angle $\varphi$ distributions for events with a small laboratory $K^-$, $\pi^-$ scattering angle $\theta_{LAB}$. The experimental distributions have been folded about the $\varphi$ 0 - 180 deg. line. The dashed histogram shows the effect of weight $W_3$ (Section IVE).

$W_3 = 1.65$ $\quad 0 \leq \beta \leq 4.5°$

$W_3 = 1.33$ $\quad 4.5 \leq \beta \leq 9°$

$W_3 = 1.0$ $\quad$ otherwise .

The result of this correction is shown in Fig. 5 as the dashed-line histograms.

For the final analysis each event was assigned a weight $W = W_1 W_2 W_3$.

## F. Consistency Checks

The lambda lifetime for a sample of 3736 of these events was found to be[29] $2.60 \pm .06 \times 10^{-10}$ sec, in good agreement with the current world average[28] of $2.51 \pm .04 \times 10^{-10}$ sec.

As a check for final-state interactions, the events were divided into forward (in the c.m.) lambdas and backward lambdas. This division should have no effect on the proton spectator distribution unless an energy-dependent final-state interaction occurs. Figure 6 shows that the spectator momentum distributions for both the forward, fast-in-the-laboratory $\Lambda$'s and the slow $\Lambda$'s are consistent with the Hulthen distribution.

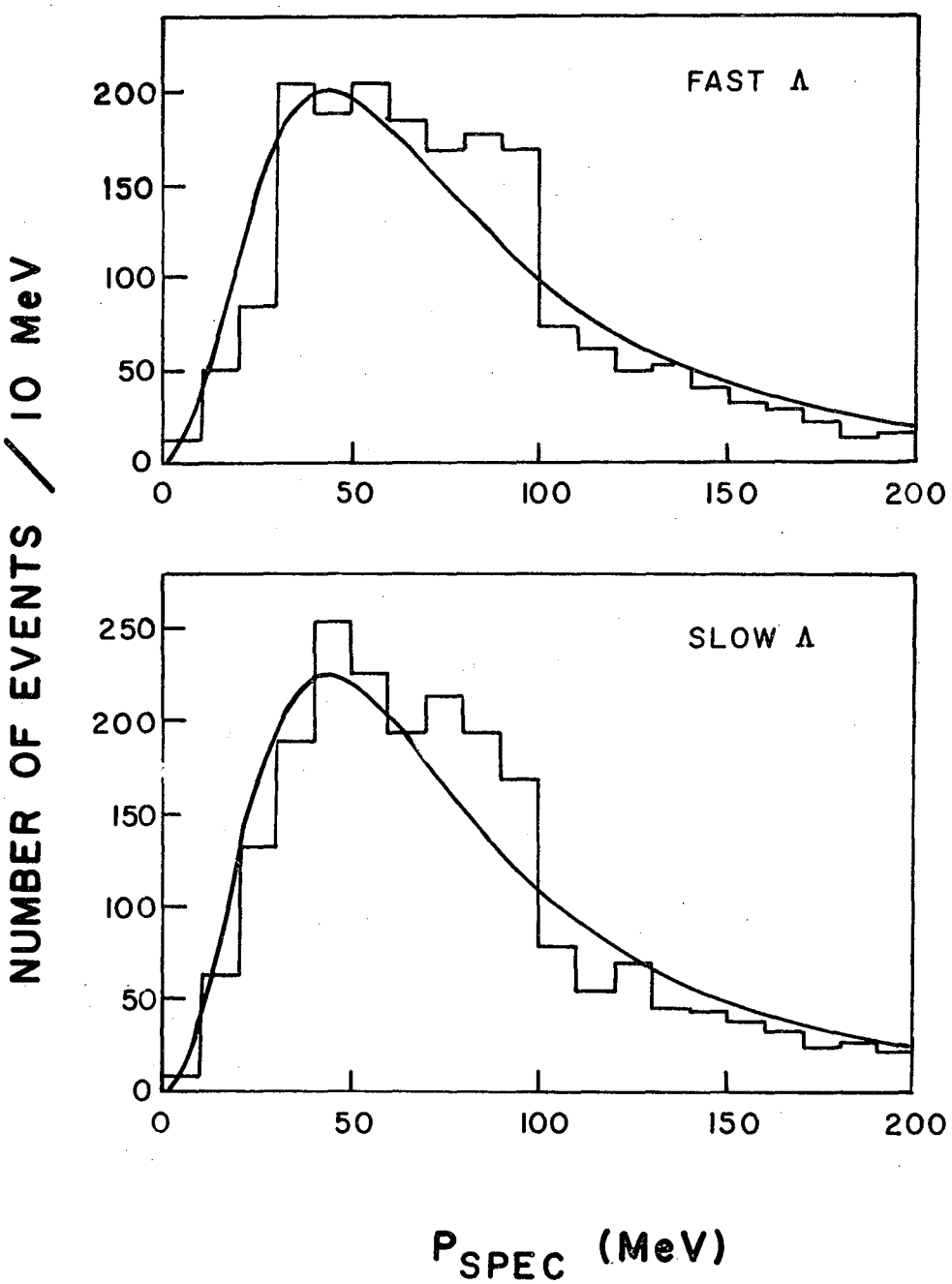


XBL 678-4487

Fig. 6. Spectator momentum distributions for fast and slow lambdas compared with the Hulthen distribution.

# V. EXPERIMENTAL RESULTS

## A. Cross Section

The cross section for $K^-n \rightarrow \Lambda\pi^-$ is just twice the cross section for $K^-n \rightarrow \Lambda\pi^\circ$ by the conservation of isotopic spin. Several measurements of the total cross section for $K^-p \rightarrow \Lambda\pi^\circ$ have been made in the energy region of this experiment,[10,30-32] and these are shown in Fig. 7, multiplied by a factor of two so they can be compared directly with the $K^-n \rightarrow \Lambda\pi^-$ cross sections.

Since accurate $K^-p \rightarrow \Lambda\pi^\circ$ cross sections existed and because of the problems associated with the Fermi momentum distribution of the neutron in the deuteron, only the average cross section at each beam momentum has been calculated. The average is over c.m. energies of ±50 MeV from the central c.m. value, corresponding to a $K^-$ of the beam momentum hitting a neutron at rest.

Table VI shows the various correction factors necessary to find the actual number of $\Lambda\pi^-$ and $\Sigma^\circ\pi^-$ events at each momentum. The number of events under the Gaussian distributions (Section IV D and Table V) were multiplied by $\bar{W}$, the average weight (Section IV E), to correct for the fiducial volume cuts and scanning biases, by 1/SE to correct for scanning efficiency, and by 1/(1-BL) to correct for bookkeeping losses. This number was multiplied by 1.045 to allow for events above the 230 MeV/c spectator momentum cutoff. This figure was obtained by integrating the Hulthen spectrum above 230 MeV/c. One further factor of 1/0.93 to correct for events lost in the $\chi^2$ cutoff (estimated in Section 4D) was applied. Finally since the branching ratio of $(\Lambda^\circ \rightarrow \pi^-p)/(\Lambda^\circ \rightarrow$ all decays) is 0.664,[28] the number of events was multiplied by 1/0.664. This corrected number of events was then

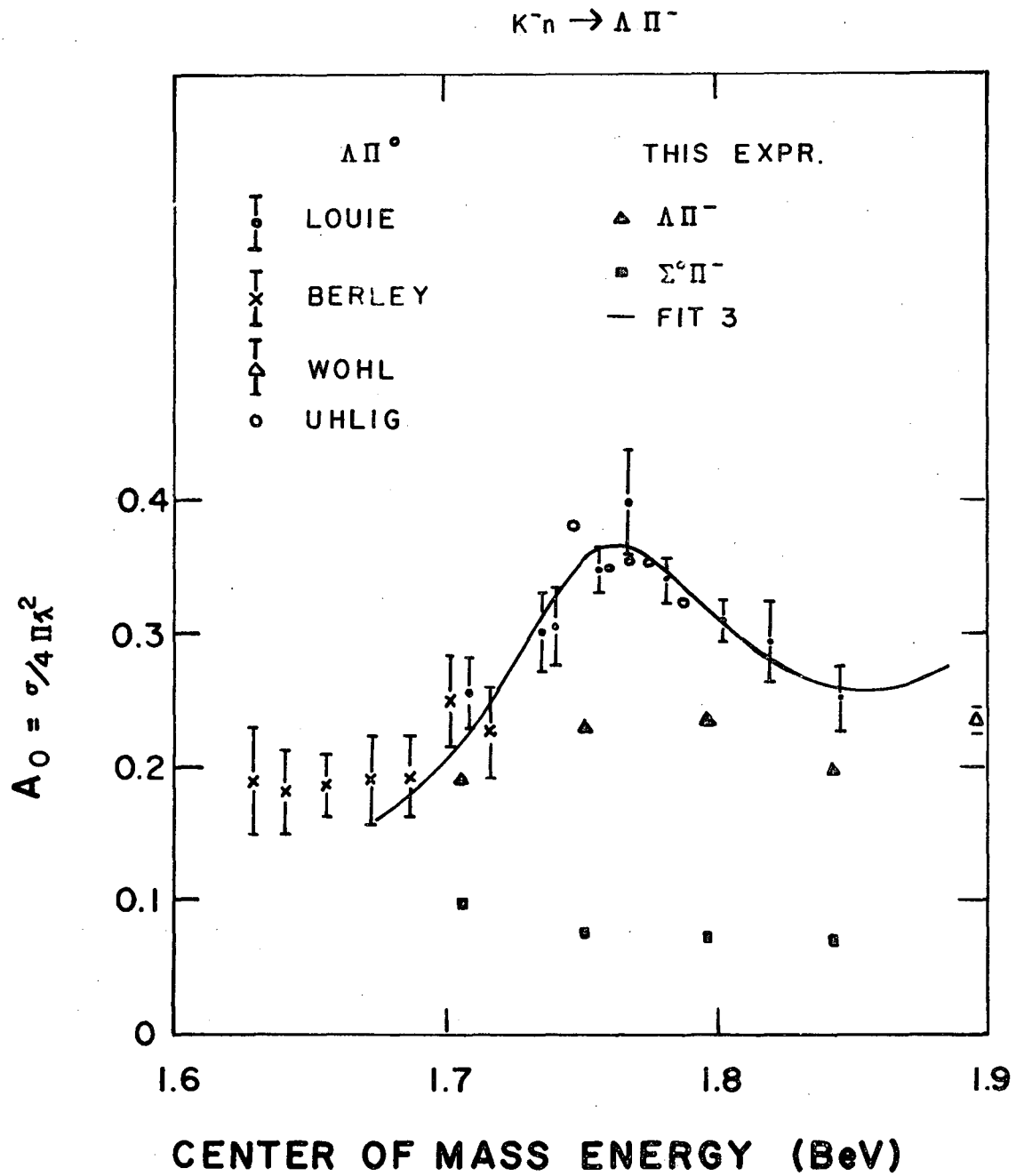


XBL 678-4488

Fig. 7. Cross sections for $K^-n \rightarrow \Lambda\pi^-$ and $K^-n \rightarrow \Sigma^\circ\pi^-$. The cross sections from this experiment are averages over ±50 MeV c.m. energy and the errors are estimated at ±15%. The curve is calculated from solution 3, described in Section VIB.

Table VI. Correction factors and cross sections for $K^-n \rightarrow \Lambda\pi^-$ and $K^-n \rightarrow \Sigma^\circ\pi^-$

| | | | | |
|---|---|---|---|---|
| Beam momentum (MeV/c) | 814 | 910 | 1007 | 1106 |
| Center of mass energy (MeV) | 1706 | 1751 | 1796 | 1843 |
| $\Lambda\pi$ events (Table V) | 355.0 | 1634.8 | 1277.4 | 1482.4 |
| $\Sigma\pi$ events (Table V) | 182.5 | 535.8 | 398.4 | 521.3 |
| Average weight, $\bar{W}$ | 1.314 | 1.344 | 1.336 | 1.310 |
| Scanning efficiency, SE (%) | 97.5 | 94.6 | 94.5 | 96.9 |
| Bookkeeping loss, BL (%) | 5.0 | 1.4 | 1.9 | 1.9 |
| Overall correction factor | 2.40 | 2.44 | 2.44 | 2.33 |
| Corrected number of $\Lambda\pi$ events | 852.2 | 3986.3 | 3115.3 | 3457.2 |
| Corrected number of $\Sigma\pi$ events | 438.1 | 1306.5 | 971.6 | 1215.7 |
| $\sigma_{\Lambda\pi}$ (mb) | 4.72 | 4.78 | 4.21 | 3.07 |
| $\sigma_{\Sigma\pi}$ (mb) | 2.43 | 1.57 | 1.31 | 1.08 |
| $4\pi\lambda\!\!\!^{-2}$ (mb) | 24.42 | 20.59 | 17.70 | 15.47 |
| $\sigma_{\Lambda\pi}/4\pi\lambda\!\!\!^{-2}$ | 1.93 | 2.32 | 2.38 | 1.99 |
| $\sigma_{\Sigma\pi}/4\pi\lambda\!\!\!^{-2}$ | 0.99 | 0.76 | 0.74 | 0.70 |

multiplied by the cross section for one event from Table IV to obtain the total cross section for $K^-n \rightarrow \Lambda\pi^-$ and $K^-n \rightarrow \Sigma^\circ\pi$ at each beam momentum.

Although the statistical errors are small the error resulting from all the correction factors was estimated at 15%. The cross sections are shown on Fig. 7 and appear in Table VI. The cross sections from this experiment are only about 80% of those expected from the $K^-p \rightarrow \Lambda\pi^\circ$ points. The source of this discrepency is unknown; however some fraction of the loss may be due to double scattering off of both the neutron and the proton.

The cross sections were plotted in units of $\sigma/4\pi\lambda\!\!\!^{-2}$, $\lambda\!\!\!^{-}$ being the incident $K^-$ c.m. wave length divided by $2\pi$. These units correspond to $A_0$, the first coefficient of the Legendre expansion, since integrating the expansion [Eq. (3)] over all angles yields

$$\sigma = 4\pi\lambda\!\!\!^{-2} A_0 .$$

B. Angular Distributions and Polarizations

For the final analysis the events were divided into ten intervals in the c.m. energy; the c.m. energy was taken as the magnitude of the constrained four-momentum of the $\Lambda\pi^-$ system. Two thirds of the events with measured spectator protons had errors in the c.m. energy of less than ±7 MeV; for unmeasured spectator events the corresponding figure was ±13 MeV.

At each energy the events were further divided into 20 intervals in the cosine of the c.m. meson scattering angle $(\hat{K} \cdot \hat{\pi}_1)$. If the actual number of events in any bin was less than ten, bins were combined until this minimum was reached. By using the total-cross-section measurements from $K^-p \rightarrow \Lambda\pi^\circ$ (shown in Fig. 7), the sum of the weights

for each bin was converted to millbarns per steradian. The fractional error for each bin was taken to be $1/\sqrt{N}$ where N is the actual number of events in the bin. Two thirds of the events with measured spectators had errors in $(\hat{K} \cdot \hat{\pi}_1)$ of less than ±.02 and for unmeasured spectators, ±.05. These differential cross sections are shown in Fig. 8 and listed in Table VII.

To obtain the Λ polarization as a function of the c.m. meson scattering angle, the events in each energy interval were redivided into bins in $(\hat{K} \cdot \hat{\pi}_1)$ having roughly 40 actual events each. For each bin the Λ polarization was calculated from the observed Λ-decay asymmetry relative to the production normal $\hat{n} = \hat{K} \times \hat{\pi}_1 / |\hat{K} \times \hat{\pi}_1|$, according to the formula $\vec{P}_\Lambda \cdot \hat{n} = (3/\alpha_\Lambda) < \hat{p} \cdot \hat{n} >$, where $\hat{p}$ is a unit vector parallel to the momentum of the proton in the Λ decay, and $\alpha_\Lambda$ is 0.66.[28] The error for each bin was calculated from $\Delta P_\Lambda = \alpha_\Lambda^{-1} \left\{ 3-(\alpha_\Lambda P_\Lambda)^2 / N \right\}^{1/2}$, where N was the number of actual events in the bin under consideration. The resulting distributions are shown in Fig. 8 and listed in Table VIII.

## C. Legendre Expansion Coefficients

It was of some interest to obtain the experimental expansion coefficients $A_m$ and $B_n$, Eq. (3). These coefficients could be used to determine the gross features of the partial waves without a complete partial-wave analysis, and they provided a convenient base to compare the solutions from a partial-wave analysis with the experimental data. Table IX gives the expansion coefficients A and B up to sixth order for each energy interval, while Figs. 9 and 10 compare the experimental A's and B's with those from various solutions of the partial-wave analysis. The coefficients have been divided by $A_0$ so that the figures show only the information learned in this experiment.

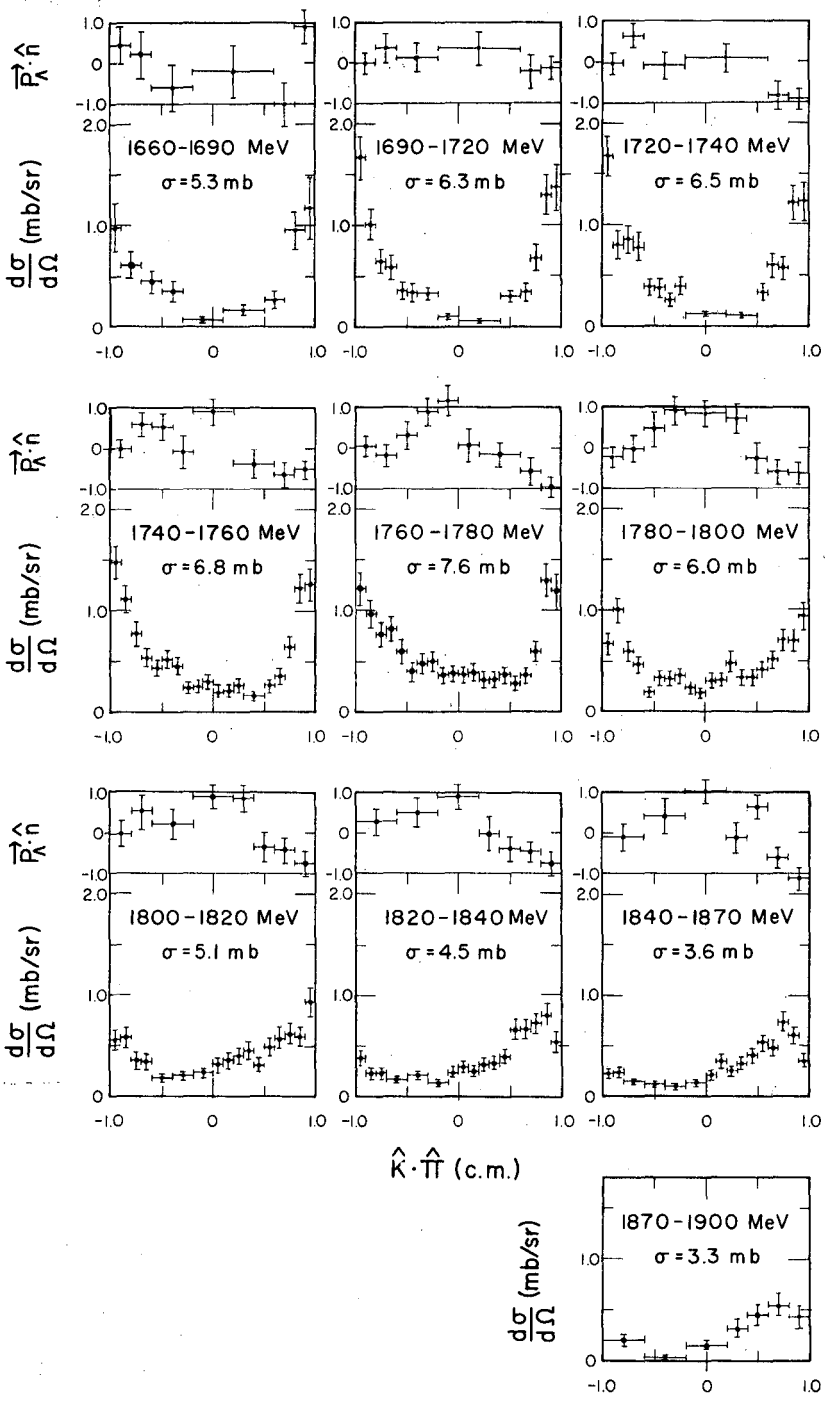


XBL 678-4493

Fig. 8. The differential cross section, $d\sigma/d\Omega$, and the lambda polarization, $P_\Lambda$, in the reaction $K^- + n \rightarrow \Lambda + \pi^-$ in the c.m. energy region 1660 to 1900 MeV.

Table VII. Differential cross sections in millibarns per steradian for $K^- n \rightarrow \Lambda \pi^-$. The angular distributions from this experiment have been normalized to twice the total cross sections for $K^- p \rightarrow \Lambda \pi^\circ$ measured by Louie.[30] The errors on the differential cross sections do not include the normalization errors.

| Center of mass energy (MeV) | 1675 | 1705 | 1730 | 1750 | 1770 |
|---|---|---|---|---|---|
| Cross section (mb) | 5.32±1.11 | 6.27±0.74 | 6.47±0.67 | 6.80±0.68 | 7.55±0.76 |
| Cos $\theta_{cm}$ | | | | | |
| -1.0 -0.9 | 0.98±.24 | 1.67±.21 | 1.68±.19 | 1.48±.16 | 1.21±.16 |
| -0.9 -0.8 | * | 1.01±.15 | 0.81±.13 | 1.11±.14 | 0.97±.14 |
| -0.8 -0.7 | 0.62±.13 | 0.65±.12 | 0.86±.13 | 0.77±.12 | 0.77±.12 |
| -0.7 -0.6 | * | 0.60±.12 | 0.79±.13 | 0.54±.09 | 0.82±.12 |
| -0.6 -0.5 | 0.45±.11 | 0.36±.09 | 0.38±.09 | 0.43±.08 | 0.60±.10 |
| -0.5 -0.4 | * | 0.33±.09 | 0.38±.09 | 0.52±.09 | 0.40±.09 |
| -0.4 -0.3 | 0.35±.10 | * | 0.26±.07 | 0.46±.09 | 0.48±.10 |
| -0.3 -0.2 | * | 0.33±.06 | 0.40±.09 | 0.24±.06 | 0.50±.10 |
| -0.2 -0.1 | 0.08±.03 | * | * | 0.25±.06 | 0.36±.08 |
| -0.1 0.0 | | 0.10±.03 | 0.11±.02 | 0.30±.07 | 0.38±.09 |
| 0.0 0.1 | * | * | | 0.21±.06 | 0.37±.08 |
| 0.1 0.2 | | 0.06±.02 | * | 0.21±.06 | 0.39±.09 |
| 0.2 0.3 | 0.17±.05 | | | 0.27±.07 | 0.32±.08 |
| 0.3 0.4 | | * | 0.11±.03 | * | 0.33±.08 |
| 0.4 0.5 | * | 0.30±.06 | * | 0.16±.04 | 0.37±.08 |
| 0.5 0.6 | 0.27±.09 | * | 0.34±.08 | * | 0.28±.07 |
| 0.6 0.7 | * | 0.34±.09 | 0.61±.12 | 0.26±.06 | 0.36±.08 |
| 0.7 0.8 | 0.96±.17 | 0.68±.13 | 0.57±.11 | 0.35±.08 | 0.60±.10 |
| 0.8 0.9 | * | 1.29±.19 | 1.21±.17 | 0.65±.10 | 1.30±.16 |
| 0.9 1.0 | 1.18±.30 | 1.38±.21 | 1.23±.19 | 1.21±.15 | 1.19±.17 |
| | | | | 1.26±.17 | |

Table VII. Continued

| Center of mass energy (MeV) | 1790 | 1810 | 1830 | 1855 | 1885 |
|---|---|---|---|---|---|
| Cross section (mb) | 5.95±0.45 | 5.11±0.43 | 4.45±0.48 | 3.59±0.45 | 3.25±0.69 |
| Cos $\theta_{cm}$ | | | | | |
| -1.0 -0.9 | 0.68±.10 | 0.56±.10 | 0.38±.07 | 0.23±.05 | * |
| -0.9 -0.8 | 1.01±.13 | 0.58±.10 | 0.23±.05 | 0.24±.06 | |
| -0.8 -0.7 | 0.60±.10 | 0.36±.08 | 0.23±.06 | * | 0.21±.05 |
| -0.7 -0.6 | 0.47±.08 | 0.34±.07 | * | 0.15±.03 | |
| -0.6 -0.5 | 0.19±.05 | * | 0.17±.03 | * | * |
| -0.5 -0.4 | 0.33±.07 | 0.18±.04 | * | 0.12±.03 | |
| -0.4 -0.3 | 0.33±.07 | * | 0.21±.04 | * | 0.05±.02 |
| -0.3 -0.2 | 0.36±.07 | 0.21±.04 | * | 0.11±.03 | |
| -0.2 -0.1 | 0.25±.06 | * | 0.14±.03 | * | * |
| -0.1 0.0 | 0.19±.05 | 0.24±.04 | * | 0.14±.03 | |
| 0.0 0.1 | 0.31±.07 | 0.32±.07 | 0.23±.06 | * | 0.16±.05 |
| 0.1 0.2 | 0.31±.07 | 0.36±.08 | 0.29±.06 | 0.21±.05 | |
| 0.2 0.3 | 0.48±.08 | 0.40±.08 | 0.25±.06 | 0.35±.07 | * |
| 0.3 0.4 | 0.34±.07 | 0.46±.08 | 0.32±.07 | 0.25±.05 | 0.32±.09 |
| 0.4 0.5 | 0.34±.08 | 0.31±.07 | 0.33±.07 | 0.33±.06 | * |
| 0.5 0.6 | 0.42±.08 | 0.49±.09 | 0.39±.07 | 0.40±.07 | 0.45±.10 |
| 0.6 0.7 | 0.52±.09 | 0.58±.10 | 0.66±.10 | 0.53±.08 | * |
| 0.7 0.8 | 0.71±.11 | 0.62±.10 | 0.66±.10 | 0.48±.08 | 0.55±.11 |
| 0.8 0.9 | 0.70±.11 | 0.59±.10 | 0.73±.10 | 0.73±.09 | * |
| 0.9 1.0 | 0.94±.14 | 0.94±.15 | 0.81±.11 | 0.60±.09 | 0.43±.11 |
| | | | 0.54±.10 | 0.34±.07 | * |

Table VIII. Polarization of the $\Lambda$ for $K^- n \rightarrow \Lambda \pi^-$.

| Center of mass energy (MeV) | | 1675 | 1705 | 1730 | 1750 | 1770 |
|---|---|---|---|---|---|---|
| Cos $\theta_{cm}$ | | | | | | |
| -1.0 | -0.8 | 0.44±.46 | 0.01±.25 | -0.02±.25 | 0.01±.21 | 0.04±.25 |
| -0.8 | -0.6 | 0.22±.58 | 0.38±.35 | 0.65±.28 | 0.59±.30 | -0.17±.28 |
| -0.6 | -0.4 | * | * | * | 0.54±.33 | 0.32±.35 |
| -0.4 | -0.2 | -0.61±.56 | 0.12±.34 | -0.08±.32 | -0.07±.39 | 0.92±.34 |
| -0.2 | 0.0 | * | * | * | * | 1.17±.38 |
| 0.0 | 0.2 | | | | 0.93±.31 | 0.07±.41 |
| 0.2 | 0.4 | -0.20±.65 | 0.34±.40 | 0.09±.36 | * | * |
| 0.4 | 0.6 | | | | -0.37±.36 | -0.15±.31 |
| 0.6 | 0.8 | * | * | * | * | * |
| 0.8 | 1.0 | -1.00±.52 | -0.21±.40 | -0.82±.34 | -0.66±.33 | -0.58±.35 |
| | | 0.91±.42 | -0.12±.28 | -0.90±.25 | -0.52±.23 | -0.98±.23 |

Table VIII. Continued

| Center of mass energy (MeV) Cos $\theta_{cm}$ | 1790 | 1810 | 1830 | 1855 |
|---|---|---|---|---|
| -1.0 -0.8 | -0.22±.25 | 0.00±.32 | * | * |
| -0.8 -0.6 | -0.01±.31 | 0.56±.40 | 0.30±.30 | -0.10±.33 |
| -0.6 -0.4 | 0.47±.43 | * | * | * |
| -0.4 -0.2 | 0.92±.36 | 0.23±.38 | 0.53±.37 | 0.42±.42 |
| -0.2 0.0 | * | * | * | * |
| 0.0 0.2 | 0.86±.29 | 0.91±.29 | 0.91±.30 | 1.03±.29 |
| 0.2 0.4 | * | * | * | * |
| 0.4 0.6 | 0.73±.34 | 0.87±.33 | -0.02±.39 | -0.13±.37 |
| 0.6 0.8 | -0.25±.38 | -0.34±.36 | -0.40±.30 | 0.65±.29 |
| 0.8 1.0 | -0.59±.29 | -0.42±.30 | -0.46±.26 | -0.61±.25 |
| | -0.63±.27 | -0.73±.29 | -0.76±.28 | -1.12±.28 |

Table IX. Coefficients, $A_m$, from the least-squares fits of the differential cross sections to the Legendre series $I = d\sigma/d\Omega = \lambda\!\!\!^{-2} \sum_{m=0} A_m P_m (\cos\theta)$, and $B_n$, from the least-squares fits of the polarization of the Legendre series

$$I\vec{P} = \hat{n}\lambda\!\!\!^{-2} \sum_{n=1} B_n P_n^1 (\cos\theta)$$

for fourth, fifth, and sixth order. The coefficients have been normalized by dividing by $A_0 = \sigma/4\pi\lambda\!\!\!^{-2}$. The confidence level in percent is given for each fit.

| Energy (MeV) | Confid. level (%) | $A_1/A_0$ | $A_2/A_0$ | $A_3/A_0$ | $A_4/A_0$ | $A_5/A_0$ | $A_6/A_0$ |
|---|---|---|---|---|---|---|---|
| 1675 | 19 | 0.11±.20 | 1.82±.27 | 0.35±.26 | 0.15±.30 | | |
| | 14 | 0.13±.20 | 1.82±.26 | 0.46±.30 | 0.19±.30 | 0.25±.34 | |
| | 10 | 0.12±.20 | 1.82±.26 | 0.49±.30 | 0.34±.34 | 0.20±.34 | 0.39±.42 |
| 1705 | 12 | -0.09±.12 | 2.07±.16 | 0.32±.15 | 0.52±.18 | | |
| | 18 | -0.13±.12 | 2.05±.16 | 0.14±.19 | 0.53±.18 | -0.27±.18 | |
| | 28 | -0.14±.12 | 2.07±.16 | 0.13±.19 | 0.72±.21 | -0.29±.18 | 0.41±.23 |
| 1703 | 4 | -0.16±.11 | 1.87±.14 | 0.29±.14 | 0.40±.16 | | |
| | 7 | -0.19±.11 | 1.85±.14 | 0.11±.16 | 0.37±.15 | -0.36±.19 | |
| | 5 | -0.19±.11 | 1.85±.14 | 0.11±.17 | 0.41±.20 | -0.37±.20 | 0.06±.19 |
| 1750 | 47 | -0.19±.09 | 1.60±.12 | 0.24±.12 | 0.68±.13 | | |
| | 41 | -0.20±.09 | 1.59±.12 | 0.21±.14 | 0.68±.13 | -0.06±.15 | |
| | 35 | -0.20±.09 | 1.59±.12 | 0.21±.14 | 0.65±.15 | -0.06±.15 | -0.07±.17 |
| 1770 | 45 | -0.15±.08 | 1.07±.11 | 0.25±.12 | 0.51±.13 | | |
| | 47 | -0.13±.09 | 1.08±.11 | 0.31±.13 | 0.50±.13 | 0.16±.15 | |
| | 43 | -0.14±.09 | 1.07±.11 | 0.31±.13 | 0.46±.15 | 0.17±.15 | -0.12±.17 |
| 1790 | 1 | 0.16±.09 | 0.97±.11 | -0.11±.12 | 0.23±.13 | | |
| | 1 | 0.17±.09 | 0.97±.11 | -0.07±.13 | 0.25±.13 | 0.16±.16 | |
| | 2 | 0.15±.09 | 0.97±.11 | -0.08±.13 | 0.14±.15 | 0.14±.16 | -0.29±.18 |
| 1810 | 60 | 0.39±.09 | 0.81±.12 | -0.24±.13 | 0.29±.15 | | |
| | 65 | 0.40±.09 | 0.82±.12 | -0.17±.14 | 0.33±.16 | 0.23±.18 | |
| | 65 | 0.40±.09 | 0.80±.12 | -0.18±.15 | 0.27±.17 | 0.20±.18 | -0.17±.19 |
| 1830 | 26 | 0.77±.09 | 0.63±.11 | -0.26±.13 | -0.21±.14 | | |
| | 62 | 0.77±.09 | 0.65±.11 | -0.35±.13 | -0.32±.15 | -0.39±.16 | |
| | 57 | 0.78±.09 | 0.65±.11 | -0.34±.13 | -0.35±.16 | -0.41±.17 | -0.12±.19 |
| 1855 | 30 | 0.80±.09 | 0.46±.11 | -0.55±.12 | -0.38±.14 | | |
| | 42 | 0.81±.09 | 0.49±.11 | -0.59±.13 | -0.45±.15 | -0.24±.16 | |
| | 60 | 0.82±.09 | 0.51±.11 | -0.57±.13 | -0.52±.15 | -0.33±.17 | -0.35±.19 |
| 1885 | 80 | 0.83±.19 | 0.66±.24 | -0.90±.28 | -0.26±.43 | | |
| | 100 | 0.81±.20 | 0.73±.28 | -1.08±.48 | -0.08±.58 | -0.48±1.03 | |

Table IX. Continued

| Energy (MeV) | Confid. level (%) | $B_1/A_0$ | $B_2/A_0$ | $B_3/A_0$ | $B_4/A_0$ | $B_5/A_0$ | $B_6/A_0$ |
|---|---|---|---|---|---|---|---|
| 1675 | 1 | -0.13± .22 | -0.05± .23 | 0.12± .22 | -0.13± .18 | | |
| | 12 | -0.07± .22 | -0.25± .24 | -0.02± .22 | 0.15± .21 | 0.71± .27 | |
| 1705 | 84 | 0.09± .12 | -0.14± .13 | -0.01± .13 | -0.08± .11 | | |
| | 79 | 0.08± .12 | -0.12± .14 | -0.01± .13 | -0.11± .13 | -0.06± .18 | |
| 1730 | 6 | -0.10± .12 | -0.46± .13 | -0.18± .12 | -0.31± .11 | | |
| | 30 | -0.13± .12 | -0.37± .13 | -0.15± .12 | -0.42± .12 | -0.31± .16 | |
| 1750 | 32 | 0.10± .10 | -0.37± .10 | -0.16± .08 | -0.14± .08 | | |
| | 20 | 0.10± .10 | -0.37± .10 | -0.16± .09 | -0.13± .08 | 0.00± .07 | |
| | 13 | 0.10± .10 | -0.36± .10 | -0.16± .09 | -0.11± .09 | 0.00± .07 | 0.07± .08 |
| 1770 | 5 | 0.10± .11 | -0.29± .10 | -0.31± .08 | -0.03± .08 | | |
| | 4 | 0.08± .11 | -0.29± .10 | -0.35± .09 | -0.03± .08 | -0.10± .07 | |
| | 90 | 0.06± .11 | -0.32± .10 | -0.37± .09 | -0.12± .08 | -0.12± .07 | -0.23± .07 |
| 1790 | 73 | 0.16± .11 | -0.22± .10 | -0.34± .08 | -0.06± .08 | | |
| | 79 | 0.14± .11 | -0.22± .10 | -0.38± .09 | -0.07± .08 | -0.07± .07 | |
| | 65 | 0.15± .11 | -0.21± .10 | -0.38± .09 | -0.07± .08 | -0.07± .07 | 0.02± .07 |
| 1810 | 45 | 0.20± .13 | -0.26± .11 | -0.32± .10 | -0.25± .09 | | |
| | 29 | 0.20± .13 | -0.26± .11 | -0.32± .10 | -0.25± .09 | -0.01± .08 | |
| | 31 | 0.20± .13 | -0.26± .11 | -0.32± .10 | -0.23± .09 | -0.01± .08 | 0.10± .09 |
| 1830 | 79 | 0.02± .13 | -0.41± .12 | -0.34± .10 | -0.14± .09 | | |
| | 69 | 0.01± .13 | -0.41± .12 | -0.33± .10 | -0.13± .09 | 0.04± .09 | |
| | 43 | 0.00± .13 | -0.39± .12 | -0.33± .10 | -0.15± .09 | 0.08± .10 | -0.13± .15 |
| 1855 | 2 | 0.09± .13 | -0.27± .11 | -0.45± .10 | -0.22± .08 | | |
| | 1 | 0.11± .14 | -0.25± .11 | -0.45± .10 | -0.24± .08 | -0.09± .09 | |
| | 1 | 0.10± .14 | -0.20± .12 | -0.45± .10 | -0.27± .08 | -0.01± .10 | -0.24± .15 |

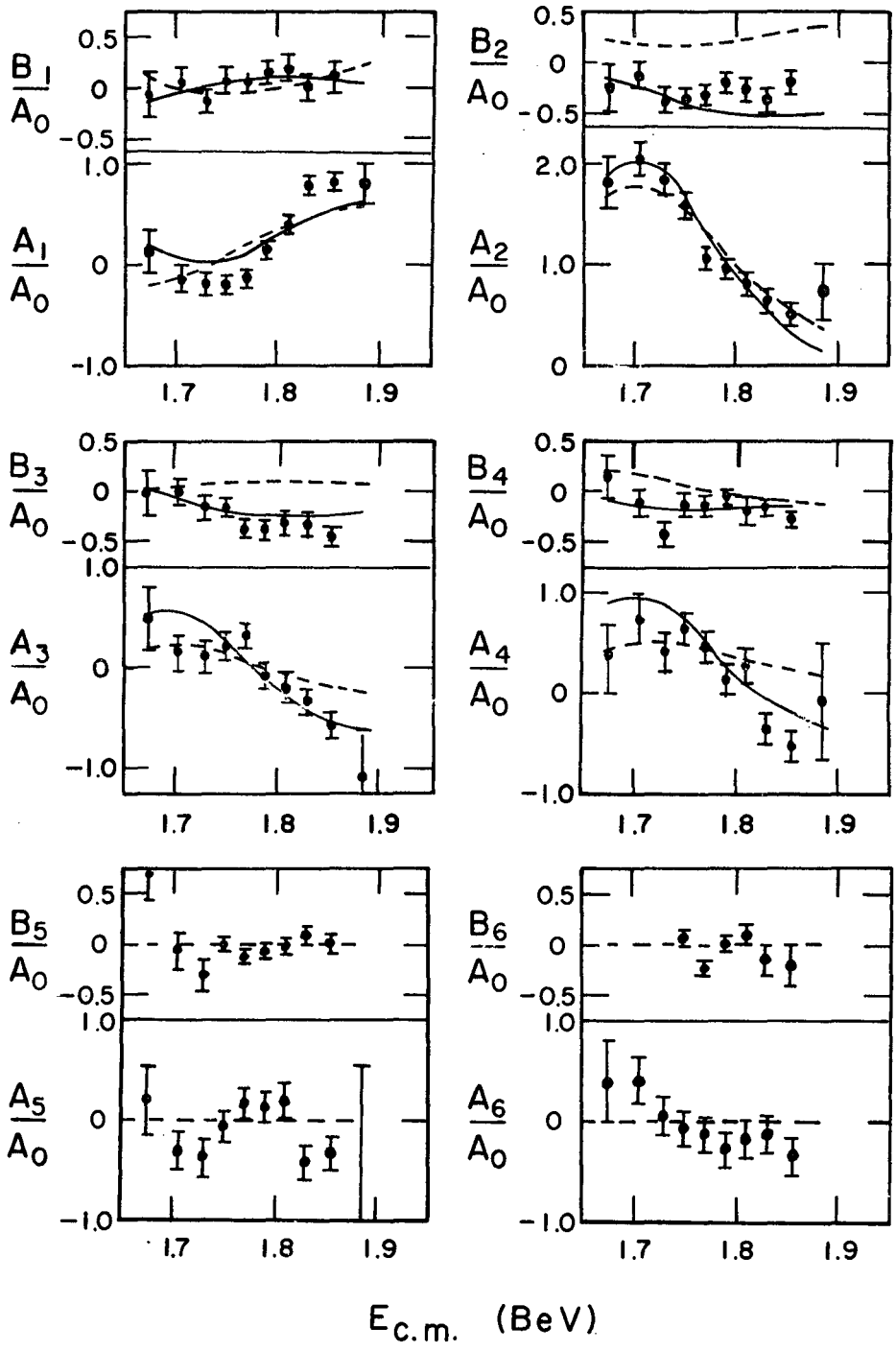


XBL 678-4489

Fig. 9. Coefficients $A_i/A_0$ and $B_i/A_0$ obtained by fitting the angular and polarization distributions in Fig. 8 with the expansions (3). The continuous curves are calculated from solution 1a, with resonant $D_5$ amplitude; the dashed curves correspond to solution 1b, with resonant $F_5$ amplitude.

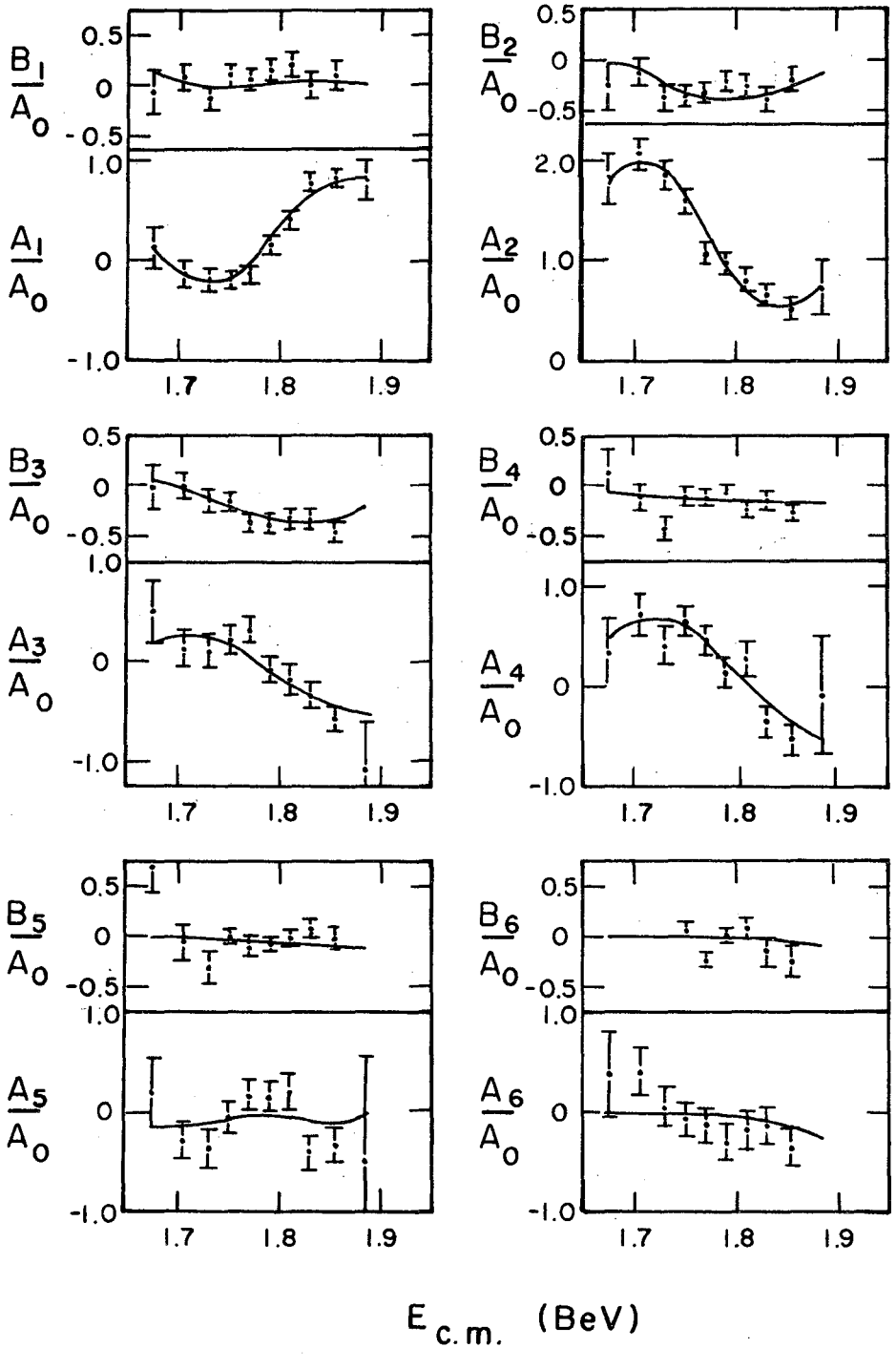


XBL 678-4490

Fig. 10. Coefficients $A_i/A_0$ and $B_i/A_0$. The curves are calculated from solution 3.

# VI. PARTIAL-WAVE ANALYSIS

## A. πN Methods, Assumptions, and Fitting Procedure

In order to study in detail any $Y_1^*$ resonant amplitudes in the reaction $K^-n \to \Lambda\pi^-$ it was necessary to decompose the amplitudes into eigenstates of angular momentum and parity, i.e. partial-wave amplitudes, and to identify those partial-wave amplitudes which had the resonant Breit-Wigner dependence with energy:

$$T = \frac{e^{i\varphi}(x_{N\bar{K}}-x_{\Lambda\pi})^{1/2}\,\Gamma/2}{E_R - E - i\,\Gamma/2} \quad . \tag{11}$$

Here $\varphi$ is the phase angle of the resonant amplitude at resonance energy; for $\varphi = 0$ the amplitude is pure positive imaginary at resonance.

The problem of all partial-wave analyses is, given the experimental distributions I and $\vec{P}$, to solve Eqs. (1) and (2)

$$a(\theta) = \lambda \sum_\ell \left[(\ell+1)\,T_\ell^{+} + \ell T_\ell^{-}\right] P_\ell(\cos\theta) \tag{1a}$$

$$b(\theta) = i\lambda \sum_\ell \left[T_\ell^{+} - T_\ell^{-}\right] P_\ell^{1}(\cos\theta) \tag{1b}$$

$$I = \frac{d\sigma}{d\Omega} = |a|^2 + |b|^2 \tag{2a}$$

$$I\vec{P} = 2\,\mathrm{Re}\,(a^* b)\,\hat{n} \tag{2b}$$

for the partial-wave amplitudes $T_\ell^{\pm}$. This is a problem in nonlinear least-squares minimization and requires rather sophisticated computer programs and considerable computer time to solve. If one knew all the $T_\ell^{\pm}$ values at a particular energy, it would be a simple matter to use these values in Eq. (1) to find $a(\theta)$ and $b(\theta)$ and then obtain I and $I\vec{P}$ from Eq. (2).

The large amount of accurate data in the $\pi N$ elastic and charge-exchange channels has permitted several authors to publish detailed phase-shift analyses up to c.m. energies of 1600 MeV. These analyses differ basically in the method used to ensure smooth energy dependence of the phase shifts and absorption parameters as a function of c.m. energy in the absence of any general theory for this dependence. Roper[33] used a power-series expansion in k (the c.m. momenta), plus Breit-Wigner resonance amplitudes. Bransden[34] uses a different parameterization based on dispersion relations and the analytic properties of the partial-wave amplitudes. Bareyre[35] finds a unique solution by fitting data at each energy separately and then selecting the solution that joins smoothly to the lower-energy solution. Auvil[36] and Donnachie[37] require smooth behavior of single energy solutions plus dispersion-relation calculations for the smaller partial waves.

All these phase-shift analyses used two advantages of the $\pi N$ elastic problem not available in the inelastic reaction $K^- n \rightarrow \Lambda \pi^-$. The optical theorem

$$\text{Im } a\ (0) = \frac{k}{4\pi}\ \sigma_\tau \quad .$$

removes the phase ambiguity from each energy solution in the elastic channel. To match the phase of solutions at different energies in an inelastic channel requires an assumption for the energy dependence of one partial wave. The $\pi N$ channels have accurate data for a wide c.m. energy range, from threshold to at least 1600 MeV, permitting a smooth continuation of the less complex low-energy solution to higher energies where $\ell = 3$ or 4 amplitudes are required.

To do a partial-wave analysis on the data of this experiment the energy behavior of each amplitude was parameterized and then all the

data fitted together. This procedure overcame the two difficulties discussed above and also insured that the Wigner condition was obeyed. This was basically Roper's[33] approach, but far few parameters for energy dependence were required to adequately fit the $K^-n \to \Lambda\pi^-$ data. The partial waves were parameterized as either Breit-Wigner resonances, Eq. (11), with the possibility of varying $\varphi$, $(x_{N\bar{K}}\, x_{\Lambda\pi})^{1/2}$, $\Gamma$, and $E_R$, or as constant nonresonant amplitudes

$$T = Ae^{iC} \tag{12}$$

with A and C variable. For each fit a hypothesis was made as to which partial waves were resonant [Eq. (11)]. The lower partial waves were approximated by Eq. (12). A set of parameters was chosen to describe each hypothesis and reasonable starting values guessed for each parameter. These starting values were used to calculate the cross sections, angular distributions, and polarizations. The calculated quantities $x_i^c$ were compared with the observed data points $x_i^o$ and their errors $\Delta x_i^o$ to find $\chi^2$:

$$\chi^2 = \Sigma \left( \frac{x_i^c - x_i^o}{\Delta x_i^o} \right)^2 ,$$

where the index i runs over all the experimental data points. For this experiment the data points were the polarizations and the shapes of the angular distributions from $K^-n \to \Lambda\pi^-$, shown in Fig. 8, and the total cross sections for $K^-n \to \Lambda\pi^-$ calculated from the experimentally measured cross sections for $K^-p \to \Lambda\pi^\circ$ (Fig. 7). The $\chi^2$ function was then minimized with respect to all the parameters by the variable metric method[38] using the program VARMIT written at LRL by Beals.[39]

VARMIT is a general fitting program for determining the local

minimum of a function of many parameters. It requires the calculation of the analytic partial derivatives of the function with respect to each parameter. It then uses an iterative procedure to find a local minimum of the function. At each iteration the minimizing program was supplied with the value of $\chi^2$ and the analytic derivatives of $\chi^2$ with respect to each parameter. These partial derivatives define a gradient direction for the most rapid variation of $\chi^2$. A matrix containing approximate second partial-derivative information was used to modify the gradient direction. In this modified direction the $\chi^2$ and gradient values of another point were calculated. Then a $\chi^2$ minimum in this direction was found by using a cubic approximation. A quadric approximation to the second derivatives in this direction was used to correct the matrix, and a new iteration was started.

After a satisfactory minimum was obtained, the values of the parameters were displaced randomly from their minimum values, and the above procedure was repeated as a consistency check. Approximately 2 minutes were required to complete a fit for 15 parameters to 200 data points on the CDC 6600 computer if a reasonable set of starting values was chosen. Ten minutes per fit were required on the IBM 7094 Mark II computer.

After solutions have been obtained for several different parameterizations, the $\chi^2$ values for each can be compared, and parameterizations that do not fit the experimental data can be rejected. This was usually done by computing the confidence level,

$$CL \simeq (2\pi)^{-1/2} \int_t^\infty e^{-y^2/2}\, dy \; ; \; t = (2\chi^2)^{1/2} - (2n-1)^{1/2} \; ,$$

which is the probability that another experiment would give a worse

fit, assuming that the parameterization accurately described the actual situation. Here n is the number of degrees of freedom, i.e. the number of independent data points minus the number of free parameters. The equation is valid for $n > 30$.

A potential problem in any nonlinear least-squared minimization problem is that any method of solution finds only local minima, i.e. the solution nearest to the starting value. A grid search over the hyperspace of the parameters is not practical; to try 10 values for each of 11 parameters would involve $10^{11}$ calculations of the $\chi^2$ function. There exists a searching program, MINFUN,[40] which explores the valleys in the $\chi^2$ hypersurface. This search routine has been used to increase our confidence in the uniqueness of a solution, but it cannot absolutely rule out the existence of other solutions.

The major drawback to this procedure was that the constraints of the chosen parameterization might bias the results. This has been checked by trying several spin-parity assignments for various resonances and by adding energy-dependent parameters to the nonresonant amplitudes to measure any effect on the value of the resonant parameters. The conclusion was that any such bias has not shifted any quantity by more than its error as listed in Table X.

## B. Results of the Phase-Shift Analysis

The $K^- p \to \Lambda\pi^\circ$ cross section shows a broad peak centered about 1770 MeV over a substantial background (Fig. 7), suggesting the presence of $Y_1^*(1765)$ plus slowly varying backgrounds. The first step in the partial-wave analysis was to test for the presence of $Y_1^*(1765)$ with $J = 5/2$ in the $\Lambda\pi$ channel. In fit 1a a single $5^-/2$ (D-wave) resonant amplitude [Eq. (11)] was hypothesized; in fit 1b a $5^+/2$ (F-wave)

Table X. Parameters and quantum numbers of $Y_1^*(1660)$, $Y_1^*(1765)$, $Y_1^*(1915)$, and $Y_1^*(2030)$. The quantities measured or verified in this experiment are underlined with a solid line; quantities suggested by this experiment are indicated by a broken line.

| Mass $E_R$ (MeV) | Width $\Gamma$ (MeV) | Spin J | Parity P | $x_{KN}x_{\Lambda\pi}$ | $x_{KN}$ | $x_{\Lambda\pi}$ | $\Phi$ (deg) |
|---|---|---|---|---|---|---|---|
| 1660 | 50 | 3/2 | - | 0.012±.015 | 0.15 | 0.08±.10 | 205±22 |
| 1772±6 | 129±17 | 5/2 | - | 0.076±.009 | 0.49 | 0.15±.02 | 0 |
| 1915 | 65 | 5/2 | + | 0.013±.009 | 0.08 | 0.16±.12 | 9±18 |
| 2035 | 160 | 7/2 | + | 0.128±.048 | 0.16 | 0.80±0.30 | 163±9 |

resonance was tried instead. No general theory exists for the energy dependence of nonresonant partial-wave amplitudes; for fits 1 through 4 we simply assumed they were independent of energy. In fits 1, 2, and 3, the four lowest-partial-wave amplitudes, S1, P1, P3, and D3 were parameterized by Eq. (12). Aside from the resonances, the higher partial waves were assumed to be zero. Table XI lists the sets of amplitudes assumed in different fits.

The mass $E_R$, width $\Gamma$, and the magnitude of the resonant energy $x_{N\bar{K}}\, x_{\Lambda\pi} = (\Gamma_{N\bar{K}}\, \Gamma_{\Lambda\pi})/(\Gamma^2)$ of the $J = 5/2$ resonant amplitude were allowed to vary in fits 1a and 1b, for a total of 11 parameters. In both fits the overall phase ambiguity was removed by defining $\varphi = 0$ for the $J = 5/2$ resonant amplitude. This convention was followed in all fits.

The solutions that minimize $\chi^2$ for the 1a and 1b hypotheses are shown in Fig. 11a and b, and the final $\chi^2$ is listed in Table XI. The resonant D5 amplitude is clearly favored by the relative $\chi^2$ values over the resonant F5 amplitude. Although both sets of amplitudes in fit 1 were inadequate to fit the data as shown by the probabilities listed in Table XI, they are plotted against the experimental A and B coefficients in Fig. 9 to show how the polarization data, via the $B_2/A_0$ and $B_3/A_0$ coefficients, discriminates against the $5^+/2$ hypothesis and removes the ambiguity discussed in Section 2A

To check the uniqueness of solution 1a, the search mode of the program MINFUN was used to look for low regions in the 11- variable hypersurface. A total of 25 low points were used as starting values for the program VARMIT. In all cases the same solution (Fig. 11a) was obtained. The next step, fit 2, was to add a $J = 7/2$ resonant amplitude due to $Y_1^*(2030)$ to the fit 1 amplitudes. According to

Table XI. Partial-wave amplitudes used for a least-squares fit to the experimental distributions in Fig. 8. The $\chi^2$ for each fit and the corresponding probability are also listed.

| Fit | Constant amplitudes | Resonant amplitudes | $\chi^2$ | Degrees of freedom | Probability |
|---|---|---|---|---|---|
| 1a | S1,P1,P3,D3 | D5 | 385 | 209 | $10^{-13}$ |
| 1b | S1,P1,P3,D3 | F5 | 834 | 209 | $\ll 10^{-20}$ |
| 2a | S1,P1,P3,D3 | D5,F7 | 268 | 207 | 0.002 |
| 2b | S1,P1,P3,D3 | D5,G7 | 373 | 207 | $10^{-12}$ |
| 2c | S1,P1,P3,D3 | F5,F7 | 807 | 207 | $\ll 10^{-20}$ |
| 2d | S1,P1,P3,D3 | F5,G7 | 688 | 207 | $\ll 10^{-20}$ |
| 3 | S1,P1,P3,D3 | D5,F5,F7 | 250 | 205 | 0.017 |
| 4a | S1,P1,P3 | D3,D5,F7 | 172 | 128 | 0.005 |
| 4b | S1,P1,D3 | P3,D5,F7 | 198 | 128 | $4 \times 10^{-5}$ |
| 4c | S1,P1,P3,D3 | D5,F7 | 174 | 128 | 0.003 |
| | Energy dependent amplitudes | | | | |
| 5 | S1,P1,P3,D3 | D5,F5,F7 | 225 | 197 | 0.08 |

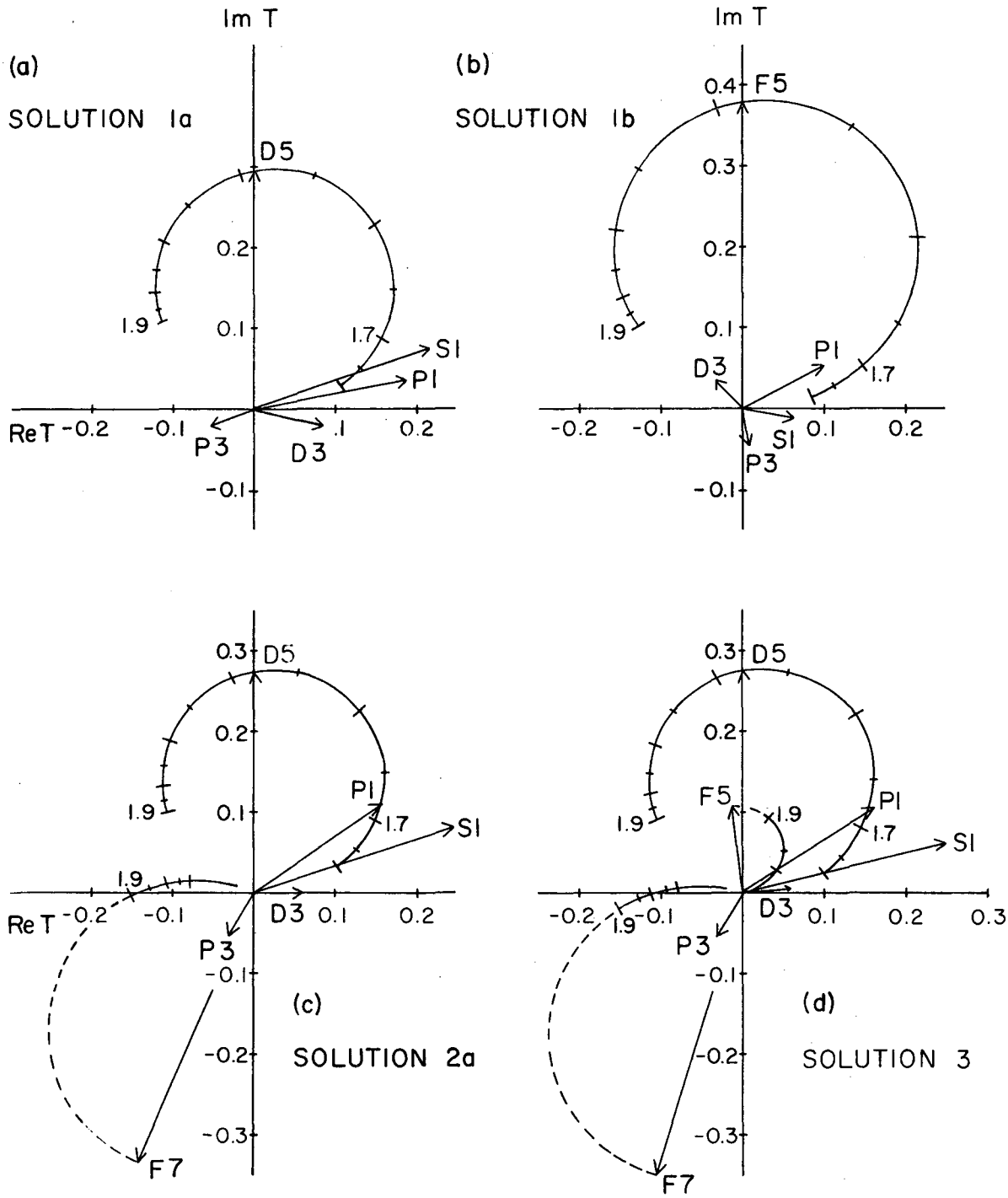


XBL 678-4492

Fig. 11. Magnitude and phases of the amplitudes which best fit the experimental data in Fig. 8 for the assumption of constant S1, P1, P3, D3 amplitudes and (a) a resonant D5 amplitude (b) a resonant F5 amplitude (c) resonant D5 and $Y_1^*(2030)$ with $J^P = 7/2^+$ or (d) resonant D5, $Y_1^*(2030)$ with $J^P = 7/2^+$, and $Y_1^*(1915)$ with $J^P = 5/2^+$.

references 9 and 10, we fixed the mass and width at 2035 MeV and 160 MeV, respectively; our data were insensitive to these parameters since the resonant energy is far removed from the energy region under study. The data were sensitive, however, to the parity of $Y_1^*(2030)$, and this was checked by trying both the $J^P = 7/2^+$ (F-wave) and $7/2^-$ (G-wave) hypotheses. The magnitude and phase of $Y^*(2030)$ were allowed to vary, thus increasing the number of variables from 11 to 13. The only acceptable solution was 2a, which requires negative parity for the $J = 5/2$ resonant amplitude and positive parity for the $J = 7/2$ resonant amplitude. Solution 2a gave 1772 ±4 and 137 ±12 MeV respectively for the mass and width of the $5/2^-$ resonance. Therefore, we identify this resonance with $Y_1^*(1765)$ and confirm the previous determination of I, $J^P = 1, 5/2^-$. This parity solution for $Y_1^*(2030)$ agrees with the measurement of Wohl, Solmitz, and Stevenson.[10] This solution is shown in Fig. 11c.

Since the I = 1 total cross section shows a shoulder which is consistent with a resonance of mass 1915 MeV and width 65 MeV,[9] a F5 resonant amplitude of this mass and width was added to solution 2a. This solution, 3, is shown in Fig. 11d and plotted against the experimental coefficients in Fig. 10. The resulting increase of probability from 0.2% to 1.7% gives some confirmation for the speculation that the total cross section shoulder is due to a resonant F5 amplitude. Further evidence that this amplitude is resonant comes from the experimental value of $\varphi = 9 \pm 18$ deg, in agreement with the requirement that $\varphi$ be 0 or 180 deg. Confirmation could come from additional $\Lambda\pi^-$ data in the region 1915 ±65 MeV,[41] which will be necessary to study this relatively weak amplitude at and above resonant energy.

Table X summarizes the parameters of $Y_1^*(1765)$, $Y_1^*(2030)$, and $Y_1^*(1915)$ determined with varying degrees of certainty in fits 2 and 3; the values quoted are the average of the results of fit 3 and the values from a similiar solution with the data box shifted 10 MeV in energy. This gives 1772 and 129 MeV respectively for the mass and the width of $Y_1^*(1765)$, together with the value of $(x_{N\bar{K}} x_{\Lambda\pi})$ for the three states. Using the published values of $x_{N\bar{K}}$, we determine the branching ratio $x_{\Lambda\pi}$ for $Y_1^*(1765)$ and $Y_1^*(1915)$ into the $\Lambda\pi$ channel. The branching ratio $x_{\Lambda\pi}$ for $Y_1^*(2030)$ is $0.80 \pm .30$, in disagreement with reference 10. The disagreement is not surprising, since it is not known whether the energy dependence assumed for $\Gamma$ is valid for energies about $2\Gamma$ below the resonant energy (Section 2A).

The errors quoted in Table X are the statistical errors calculated in our fitting program, increased by a factor of two. The statistical errors have been doubled in an attempt to include uncertainties arising from the assumptions (a) that there are no nonresonant amplitudes present with the same spin and parity as the resonances, (b) that the background amplitudes are constant, and (c) that the energy dependence used for $\Gamma$ may not be exactly correct.

Until now the $Y_1^*(1660)$ has been neglected because its amplitude in the $\Lambda\pi$ channel is weak.[28] Only the experimental data below 1800 MeV, where the $Y_1^*(1660)$ amplitude is more important, was used in fits 4 a, b, and c. One of the constant $J = 3/2$ amplitudes was replaced by a resonance of mass 1660 MeV and width 50 MeV. The magnitude and phase of the $J = 3/2$ resonance were allowed to vary. Only the $3/2^-$ resonant hypothesis led to a satisfactory fit; the corresponding $x_{N\bar{K}} x_{\Lambda\pi}$ value is given in Table XI. However, the data below 1800 MeV is almost equally well described by constant $3/2^-$ and $3/2^+$ amplitudes

as shown by fit 4c, so that the $J^P = 3/2^-$ assignment is not conclusive.

Finally, possible energy variation of nonresonant amplitudes was studied in fit 5. The parameterization

$$T = (A + Bk)\, e^{i(C + Dk)} \tag{13}$$

was used for the S1, P1, P3, and D3 amplitudes, where k is the incident c.m. momentum; A, B, C, and D were allowed to vary in the fit. With the eight addition parameters the probability of fit increases to 8.3%, but the resonance parameters agree with fit 3 within the assigned errors. These resonance parameters for fit 5 are listed in Table XII, and the Argand diagram for this solution appears as Fig. 12. The data did not really require this energy variation in the lower amplitudes, and this fit constituted a check that the earlier assumption of constant amplitudes was justified.

No general theory exists at present to explain the behavior of nonresonant partial-wave amplitudes. However this partial-wave analysis yields rough measurements of these amplitudes in the reaction $K^-n \rightarrow \Lambda\pi^-$. The A and C parameters (Eq. 12) from fit 3 for the S1, P1, P3, and D3 partial waves are listed in Table XIII. The energy dependence of these four partial waves in fit 5 is shown on Fig. 12 (solid lines). Also shown are the results of a similar fit with the data box shifted 10 MeV in energy (dashed lines). The general energy dependence of the magnitude of the S1, P1, and P3 partial waves is apparent from the figure, but the energy dependence of the phases of these three amplitudes cannot be determined from our experimental data.

Table XII. Resonance parameters for $Y_1^*(1765)$, $Y_1^*(1915)$, and $Y_1^*(2030)$ from fit 5 with energy-dependent lower partial waves.

| Mass $E_R$ (MeV) | Width $\Gamma$ (MeV) | $x_{NK}-x_{\Lambda\pi}$ | $x_{\Lambda\pi}$ | $\Phi$ (deg) |
|---|---|---|---|---|
| 1777±11 | 137±20 | 0.077±.026 | 0.16±.05 | 0 |
| 1915 | 65 | 0.013±.012 | 0.16±.15 | 33±41 |
| 2035 | 160 | 0.050±.038 | 0.31±.24 | 198±68 |

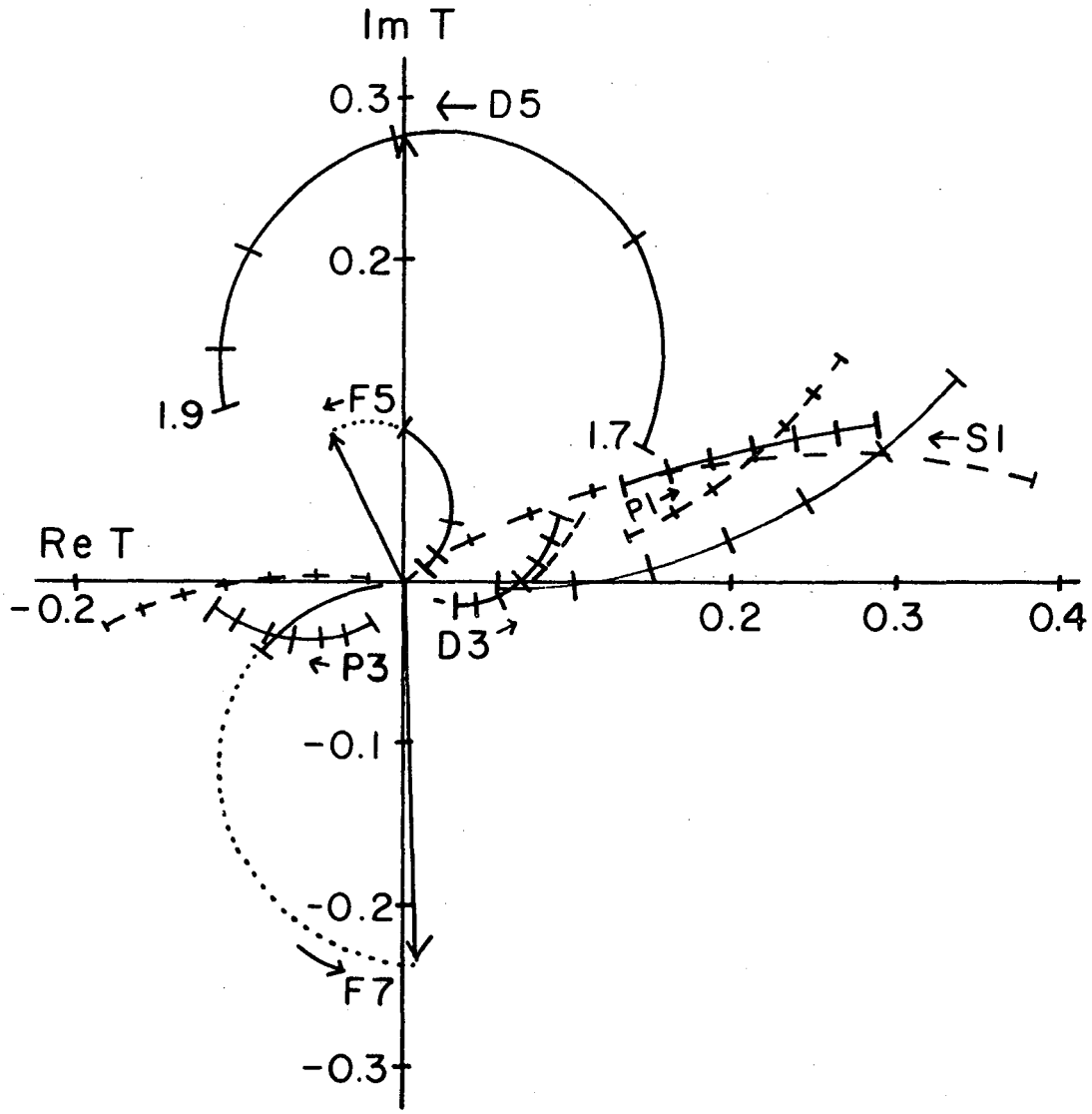


XBL 678-4491

Fig. 12. Magnitudes and phases of the amplitudes which best fit the experimental data as calculated in solution 5 with energy dependence in the lower partial waves. The continuous curves are calculated from the data as shown in Fig. 8; the dashed curves are calculated from the data box shifted 10 MeV in c.m. energy.

Table XIII. Magnitudes and phases of the nonresonant partial waves from fit 3. The amplitudes have been parameterized by

$$T = Ae^{iC}$$

| Partial Wave | A | C |
|---|---|---|
| S1 | 0.26± .02 | 0.25± .10 radian |
| P1 | 0.20± .02 | 0.56± .20 radian |
| P3 | 0.066± .011 | 4.1± .3 radian |
| D3 | 0.058± .012 | 0.1± .2 radian |

## VII. SU(3) ASSIGNMENTS

Table X lists the phase angles for $Y_1^*(1660)$, $Y_1^*(1915)$, and $Y_1^*(2030)$ relative to $Y_1^*(1765)$ as found from the partial-wave analysis. The $Y_1^*(1765)$ and $Y_1^*(1915)$ resonances are found to be in phase, but 180 deg out of phase with $Y_1^*(1660)$ and $Y_1^*(2030)$. Because of the overall phase ambiguity of partial waves in an inelastic channel, the SU(3) assignment of one resonance must be assumed in order to limit the possible assignments for the other resonances. The $Y_1^*(2030)$ has $J^P = 7^+/2$, and it has been suggested that this particle along with $\Delta(1920)$ belongs to a $7^+/2$ $\{10\}$ multiplet, which is the Regge recurrence of the $3/2^+$ $\delta$ decuplet.[10]

Table III shows that the possible SU(3) assignments for $Y_1^*$ resonances fall into two groups, depending on whether the sign of $g_{N\bar{K}Y}^* \, g_{\Lambda\pi Y}^*$ is plus or minus:

| Group I | Group II |
|---|---|
| $\{10\}$, $\{27\}$, | $\{10^*\}$, |
| $\{8\}$ with $\frac{1}{2} < \alpha < 1$ | $\{8\}$ with $\alpha < \frac{1}{2}$ or $\alpha > 1$ |

Once the assumption is made that $Y_1^*(2030)$ is a member of the $\{10\}$ multiplet, then clearly $Y_1^*(1660)$ must belong to a multiplet in group I while $Y_1^*(1765)$ and $Y_1^*(1915)$ belong in group II.

$Y_1^*(1765)$ belongs either to a $\{10^*\}$ or an octet with $\alpha < 1/2$ or $\alpha > 1$. A measurement of the relative phase of $Y_1^*(1765)$ and $Y_1^*(2030)$ in the $\Sigma\eta$ channel would resolve this ambiguity. Unfortunately the branching ratio for $Y_1^*(1765)$ decaying to $\Sigma\eta$ is probably very small because of limited phase space, since the Q value for the decay is only 30 MeV. A measurement of the relative sign of $g_{N\bar{K}Y}^* \, g_{\Sigma\pi Y}^*$ for

$Y_1^*(1765)$ and $Y_1^*(2030)$ could restrict further the value of $\alpha$ and possibly rule out $\{10^*\}$. A $\{10^*\}$ multiplet would contain a Y = 2, I = 0 resonance; evidence for this state in $K^+N$ total cross sections has been reported by Cool et al.[42] A study of the branching ratios of $Y_1^*(1765)$ by Uhlig et al.[21] favors the octet assignment with $-0.31 < \alpha < -0.1$. This is consistent with the above limits on $\alpha$. A recent comprehensive study by Tripp et al.[22] of both branching ratios and measurements of the relative signs of coupling constants, including the preliminary results of this experiment, finds $Y_1^*(1765)$ a member of an octet with $\alpha \cong -0.17$.

$Y_1^*(1915)$ also falls in group II, hence the same possible assignments are incicated as for $Y_1^*(1765)$. It has been suggested that $Y_1^*(1915)$ belongs to a $5^+/2$ octet along with $N^*(1688)$, $Y_0^*(1815)$, and possibly $\Xi^*(1933)$. This is consistent with the conclusions drawn above, the limits on $\alpha$ being less than 1/2 or greater than 1. The $1^+/2$ baryon octet has $\alpha \sim 1/4$[43,44] so the results are consistent with $\alpha$ being the same for the $1/2^+$ and $5/2^+$ baryon octets. Tripp et al.[22] find the $N\bar{K}$ and $\Lambda\pi$ branching ratios for $Y_1^*(1915)$ in fair agreement with the other members of this octet, but the experimental uppper limit for the branching ratio into $\Sigma\pi$ is nearly 100 times smaller than expected. More data is clearly needed in the 1915-MeV region in order to fully understand $Y_1^*(1915)$.

$Y_1^*(1660)$ is usually assigned to the $3^-/2$ $\gamma$ octet of baryons, and thus the $3^-/2$ $\gamma$ octet has $1/2 < \alpha < 1$.

Regardless of the $Y^*(2030)$ assignment one can still state that $\alpha$ is different for the $3/2^-$ $\gamma$ baryon octet and the proposed $5/2^+$ baryon octet. For one octet $\alpha$ lies in the range $1/2 < \alpha < 1$, and for the

other $\alpha$ is less than 1/2 or greater than 1. Cutkosky has discussed the conditions under which $\alpha$ might be the same for different baryon octets.[44]

The following reservations must be made:

(a) Most of the above conclusions are based on the assumption that $Y_1^*(2030)$ belongs to a $\{10\}$ representation. Ideally one should measure the $Y_1^*$ phase relative to $Y_1^*(1385)$, which is firmly established as a member of the $3^-/2$ baryon $\delta$ $\{10\}$.

(b) The experimental measurement of the phase of the $Y_1^*(1660)$ and $Y_1^*(1915)$ is not conclusive, because these amplitudes are relatively weak in the $\Lambda\pi$ channel, and because the data in this experiment are relatively sparse in the regions where these amplitudes are expected to be important.

## VIII. CONCLUSIONS

This partial-wave analysis of the reaction $K^- n \rightarrow \Lambda\pi^-$ has yielded considerable information on the quantum numbers, resonance parameters, and SU(3) assignments for the $Y_1^*$ resonant amplitudes present in the c.m. energy interval 1660 to 1900 MeV. A rough measurement of the nonresonant amplitudes in this reaction also resulted from the partial-wave analysis.

The $Y_1^*(1660)$ and $Y_1^*(1915)$ amplitudes are relatively weak in the $\Lambda\pi$ channel, and the experimental data in these energy regions in this experiment was rather sparse; hence only tenative information on their spin-parity assignments, $\Lambda\pi$ branching ratios, and SU(3) multiplet assignment could be obtained. Even though the $Y_1^*(2030)$ is almost a full width above the energy region of this experiment, its coupling into the $\Lambda\pi$ channel was strong enough to permit us to confirm the previous I, $J^P$ assignment of 1, $7^+/2$. The dominant feature of the $\Lambda\pi$ channel in the energy region of this experiment is the $Y_1^*(1765)$ resonance. We confirmed the previous I, $J^P$ assignment of 1, $5^-/2$ and measured the mass, width, and $\Lambda\pi$ branching ratio to be 1772 ±6 MeV, 129 ±17 MeV, and 0.15 ±.02 respectively. Assuming the $Y_1^*(2030)$ to be a member of the $\{10\}$ multiplet of SU(3), we found that $Y_1^*(1765)$ could only belong to the $\{10^*\}$ or $\{8\}$ (with $\alpha < \frac{1}{2}$ or $\alpha > 1$) multiplets of SU(3).

Finally this study has demonstrated the advantages of analyzing reaction-channel data with an energy-dependent partial-wave analysis, even with a rather modest amount of data available at each energy.

## IX. ACKNOWLEDGMENTS

I wish to thank Professor Wilson M. Powell for his support and for interesting me in High Energy Physics.

The counsel and help of Dr. Anne Kernan, Professor Robert P. Ely, and Dr. George E. Kalmus was indispensable for this experiment. The assistance of the entire Powell-Birge Physics Group, in particular James Louie and Jack S. Sahouria was extremely useful.

It is a pleasure to thank the scanners, particularly Mrs. Mattie L. Woodford and Mrs. Marleigh Sheaff, and the measurers, under the direction of P. Wesley Weber, for their work on this experiment. The Data Handling Group, headed by Howard S. White, did the data reduction. Loren Schulz assisted me in getting results from the FAIR program.

I thank Professors J. S. Ball, G. L. Shaw, K. Tanaka, and R. D. Tripp for helpful discussions. The advice of Eric R. Beals was of great assistance in solving the least-squares minimization problem.

The careful efforts of Mrs. Sandra Paciotti in typing this manuscript are greatfully acknowledged; as is the assistance of Miss Janice Chong and Miss Kimberly Erle in preparing the figures.

This work was done under the auspices of the U.S. Atomic Energy Commission and the National Science Foundation.

## X. FOOTNOTES AND REFERENCES


1. V. Cook, B. Cork, T. F. Hoang, D. Keefe, L. T. Kerth, W. A. Wenzel, and T. F. Zipf, Phys. Rev. 123, 320 (1961).
2. O. Chamberlain, K. M. Crowe, D. Keefe, L. T. Kerth, A. Lemonick, Tin Maung, and T. F. Zipf, Phys. Rev. 125, 1696 (1962).
3. A. Barbaro-Galtieri, A. Hussain, and R. D. Tripp, Phys. Letters 6, 296 (1963).
4. (a) E. F. Beall, W. Holley, D. Keefe, L. T. Kerth, J. J. Thresher, C. L. Wang, and W. A. Wenzel, in Proceedings of the 1962 International Conference on High Energy Physics at CERN, (CERN, Geneva, 1962), p. 368.
   (b) L. A. Sodickson, I. Manelli, M. Wahlig, and D. Frisch, Phys. Rev. 133, B757 (1964).
   (c) W. Graziano and S. G. Wojcicki, Phys. Rev. 128, 1868 (1962).
   (d) P. L. Bastien and J. P. Berge, Phys. Rev. Letters 10, 188 (1963).
   (e) C. Wohl, M. H. Alston, G. R. Kalbfleisch, D. H. Miller, and S. G. Wojcicki, Bull. Am. Phys. Soc. 8, 341 (1963).
5. W. M. Smart, A. Kernan, G. E. Kalmus, and R. P. Ely, Jr., Phys. Rev. Letters 17, 556 (1966).
6. A. Kernan and W. M. Smart, Phys. Rev. Letters 17, 832 (1966).
7. A. H. Rosenfeld, A. Barbaro-Galtieri, W. H. Barkas, P. L. Bastien, J. Kirz, and M. Roos, Rev. Mod. Phys. 37, 633 (1965) and Lawrence Radiation Laboratory Report UCRL-8030, August 1965.
8. (a) R. Armenteros, M. Ferro-Luzzi, D. W. G. Leith, R. Levi-Setti A. Minten, R. D. Tripp, H. Filthuth, V. Hepp, E. Kluge, H. Schneider, R. Barloutaud, P. Granet, J. Meyer, and J.-P. Porte, Phys. Letters 19, 338 (1965).

(b) R. B. Bell, R. W. Birge, Y.-L. Pan, and R. T. Pu, Phys. Rev. Letters 16, 203 (1966).

9. R. L. Cool, G. Giacomelli, T. F. Kycia, B. A. Leontić, K. K. Li, A. Lundby, and J. Teiger, Phys. Rev. Letters 16, 1228 (1966).

10. C. G. Wohl, F. T. Solmitz, and M. L. Stevenson, Lawrence Radiation Laboratory Report UCRL-16868, May 1966, and Phys. Rev. Letters 17, 107 (1966).

11. R. D. Tripp, Ann. Rev. Nucl. Sci. 15, 325 (1965). The notation of this article is followed here.

12. R. D. Tripp, Proc. International School Phys., Enrico Fermi, Varenna, Italy, course 33 (Academic Press, New York, 1966).

13. S. L. Glashow and A. H. Rosenfeld, Phys. Rev. Letters 10, 192 (1963).

14. S. R. Deans and W. G. Holladay, Bull, Am. Phys. Soc. 11, 516 (1966).

15. J. M. Blatt and V. F. Weisskopf, Theoretical Nuclear Physics (Wiley, New York, 1952), Chap. VIII; also see reference 12.

16. M. Gell-Mann, California Institute of Technology Synchrotron Laboratory Report No. CTSL 20, 1961 (unpublished) and Phys. Rev. 125, 1067 (1962).

17. Y. Ne'eman, Nucl. Phys. 26, 222 (1961).

18. G. T. Hoff, Phys. Rev. 139, B671 (1965).

19. J. J. de Swart, Rev. Mod. Phys. 35, 916 (1963).

20. P. McNamee and F. Chilton, Rev. Mod. Phys. 36, 1005 (1964).

21. R. P. Uhlig, G. R. Charlton, P. E. Condon, R. G. Glasser, G. B. Yodh, and N. Seeman, Phys. Rev. 155, 1448 (1967).

22. R. D. Tripp, D. W. G. Leith, A. Minten, R. Armenteros, M. Ferro-Luzzi, R. Levi-Setti, H. Filthuth, V. Hepp, E. Kluge, H. Schneider, R. Barloutaud, P. Granet, J. Meyer, and J. P. Porte, Lawrence Radiation Laboratory Report UCRL-17385 Rev., March 1967, and Nucl. Phys. B (to be published).

23. R. B. Bell, R. W. Bland, M. G. Bowler, J. L. Brown, R. P. Ely, S. Y. Fung, G. Goldhaber, A. A. Hirata, J. A. Kadyk, J. Louie, J. S. Sahouria, V. H. Seeger, W. M. Smart, G. H. Trilling, and C. T. Murphy, Lawrence Radiation Laboratory Report UCRL-11527, July 1964 (unpublished).

24. J. Louie and J. S. Sahouria, Lawrence Radiation Laboratory, private communication, April 1967.

25. J. D. Davies, J. D. Dowell, P. M. Hattersley, R. J. Homer, A. W. O'Dell, A. A. Carter, K. F. Riley, R. J. Tapper, D. V. Bugg, R. S. Gilmore, K. M. Knight, D. C. Salter, G. H. Stafford, and E. J. N. Wilson, Phys. Rev. Letters 18, 62 (1967).

26. J. L. Brown, Stanford Linear Accelerator Center, private communication, October 1964.

27. Reference Manuals, FOG-CLOUDY-FAIR Bubble Chamber Data Processing System, Lawrence Radiation Laboratory Report UCID-1340, 1965 (unpublished).

28. A. H. Rosenfeld, A. Barbaro-Galtieri, W. J. Podolsky, L. R. Price, P. Soding, C. G. Wohl, M. Roos, and W. J. Willis, Rev. Mod. Phys. 39, 1 (1967).

29. J. Louie, Lawrence Radiation Laboratory, private communication, December 1966.

30. R. W. Birge, R. P. Ely, G. E. Kalmus, J. Louie, A. Kernan, J. S. Sahouria, and W. M. Smart, in Proceedings of the Second Athens Topical Conference on Resonant Particles, Athens, Ohio, 1965 (University of Ohio, Athens, Ohio, 1965), p. 296, and J. Louie, Lawrence Radiation Laboratory, private communication, July 1967.

31. R. P. Uhlig, Ph.D. thesis, University of Maryland Technical Report No. 545, 1966 (unpublished).

32. D. Berley, P. L. Connolly, E. L. Hart, D. C. Rahm, D. L. Stonehill, B. Thevenet, W. J. Willis, and S. S. Yamamoto, in Proceedings of the XII International Conference on High Energy Physics, Dubna U.S.S.R., August 5-15, 1964, Vol. 1 (Atomizdat, Moscow, 1966), p. 565.

33. L. D. Roper, R. M. Wright, and B. T. Feld, Phys. Rev. 138, B190 (1965).

34. B. H. Bransden, R. G. Moorhouse, and P. J. O'Donnell, Phys. Rev. 139, B1566 (1965), and Phys. Letters 19, 420 (1965).

35. P. Bareyre, C. Bricman, A. V. Stirling, and G. Villet, Phys. Letters 18, 342 (1965).

36. P. Auvil, C. Lovelace, A. Donnachie, and A. T. Lea, Phys. Letters 12, 76 (1964).

37. A. Donnachie, R. Kirsopp, A. T. Lea, and C. Lovelace, in Proceedings of the XIII International Conference on High Energy Physics, Berkeley, California, August 31-September 7, 1966 (University of California Press, Berkeley, 1967), p. 176.

38. W. C. Davidon, "Variable Metric Minimization" Argonne National Laboratory Report ANL-5990, Rev 1959 (unpublished).

39. E. R. Beals, "Program VARMIT Writeup", LRL Computer Library Note (unpublished).

40. W. E. Humphrey, "Program MINFUN Writeup", LRL Computer Library Note (unpublished).

41. Dr. C. Wohl has kindly communicated to us the differential cross sections and polarizations for $K^- + p \rightarrow \Lambda + \pi^\circ$ at 1896-MeV c.m. energy, based on 700 events. Analysis of the combined data gives $J^P = 5/2^+$ for $Y_1^*(1915)$, with $x_{\Lambda\pi} = 0.08 \pm .04$ and $\varphi = 7 \pm 7$ deg.

When these data at 1896 MeV are added to our experimental data, the probability of obtaining a fit with constant S1, P1, P3, D3 partial waves and resonant $Y_1^*(1765)$ ($J^P = 5/2^-$) and $Y_1^*(2030)$ ($J^P = 7/2^+$) falls from 0.23% to 0.01%. Addition of an F5 ($J^P = 5/2^+$) resonant amplitude with $E_R = 1915$, $\Gamma = 65$ MeV raises the probability to 1.6%. No other spin-parity assignment for $Y_1^*(1915)$ in the range P3, D3, D5, F7, or G7 leads to a reasonable probability. After F5 the next most probable value is G7, with a probability of 0.05%. One must qualify this result by noting that the effect appears at the juncture of two different experiments in different channels with different possible experimental biases.

42. R. L. Cool, G. Giacomelli, T. F. Kycia, B. A. Leontić, K. K. Li, A. Lundby, and J. Teiger, Phys. Rev. Letters 17, 102 (1966).

43. A. W. Martin and K. C. Wali, Phys. Rev. 130, 2455 (1963).

44. R. Cutkosky, Ann. Phys. (N.Y.) 23, 415 (1963).